The immunomodulatory molecule TIGIT is expressed by chronic lymphocytic leukemia cells and contributes to anergy

haematologica
Journal of The Ferrata Storti Foundation

The immunomodulatory molecule TIGIT is expressed by chronic lymphocytic leukemia cells and contributes to anergy

by Francesca Arruga, Marta Rubin, Despoina Papazoglou, Andrea Iannello, Nikolaos Ioannou, Riccardo Moia, Davide Rossi, Gianluca Gaidano, Marta Coscia, Luca Laurenti, Giovanni D'Arena, John N. Allan, Richard R. Furman, Tiziana Vaisitti, Alan G. Ramsay, and Silvia Deaglio

Received: January 10, 2022.
Accepted: January 11, 2023.

Citation: Francesca Arruga, Marta Rubin, Despoina Papazoglou, Andrea Iannello, Nikolaos Ioannou, Riccardo Moia, Davide Rossi, Gianluca Gaidano, Marta Coscia, Luca Laurenti, Giovanni D'Arena, John N. Allan, Richard R. Furman, Tiziana Vaisitti, Alan G. Ramsay, and Silvia Deaglio. The immunomodulatory molecule TIGIT is expressed by chronic lymphocytic leukemia cells and contributes to anergy. Haematologica. 2023 Jan 19. doi: 10.3324/haematol.2022.282177 [Epub ahead of print]

Title: The immunomodulatory molecule TIGIT is expressed by chronic lymphocytic leukemia cells and contributes to anergy

Authors: Francesca Arruga[1], Marta Rubin[1], Despoina Papazoglou[2], Andrea Iannello[1], Nikolaos Ioannou[2], Riccardo Moia[3], Davide Rossi[4], Gianluca Gaidano[3], Marta Coscia[5], Luca Laurenti[6], Giovanni D'Arena[7], John N. Allan[8], Richard R. Furman[8], Tiziana Vaisitti[1], Alan G. Ramsay[2] and Silvia Deaglio[1]

Affiliations:
[1] Laboratory of Functional Genomics, Department of Medical Sciences, University of Turin, Turin, Italy;
[2] School of Cancer and Pharmaceutical Sciences, King's College London, London, United Kingdom;
[3] Division of Hematology, Department of Translational Medicine, University of Eastern Piedmont, Novara, Italy;
[4] Laboratory of Experimental Hematology, Institute of Oncology Research; Faculty of Biomedical Sciences, Università della Svizzera Italiana, Switzerland;
[5] Department of Molecular Biotechnology and Health Sciences, University of Turin and Division of Hematology, A.O.U. Città della Salute e della Scienza di Torino, Turin, Italy;
[6] Hematology Unit, IRCCS Fondazione Policlinico Gemelli, Catholic University of "Sacred Heart", Rome, Italy;
[7] Hematology, P.O. "S. Luca", ASL Salerno, Salerno, Italy.
[8] Department of Hematology, Weill Cornell Medicine, New York, NY, USA.

Running title: TIGIT axis in B-CLL cells

Text word count: 4113 words

Corresponding author: Silvia Deaglio, MD, PhD, Laboratory of Functional Genomics, Department of Medical Sciences, University of Turin, via Nizza 52, 10126 Turin, Italy. Phone (+39-011 670-9535), email: silvia.deaglio@unito.it

Conflict-of-interest: There is no conflict of interest to declare.

Data sharing: The authors adhere to the policy of data sharing.

Authors' contribution
F.A. designed the study, performed experiments, analyzed and interpreted data and together with S.D. wrote the paper; M.R., D.P. and A.I. performed experiments; R.M, D.R., G.G, M.C., L.L., G.D'A., J.N.A, R.R.F provided patient samples and relevant clinical information and contributed to data interpretation; D.P., N.I., and A.G.R. performed confocal microscopy experiments and analyses on LN tissues biopsies collected at the King's College, London; T.V. discussed results and contributed to data interpretation; S.D. designed the study, interpreted data and together with FA wrote the paper.

Acknowledgments
This work was supported by the Associazione Italiana per la Ricerca sul Cancro (AIRC IG-23095 to S.D.; My First AIRC Grant MFAG-23107 to T.V.; AIRC 5x1000 #21198 to G.G.), by the ITN INTEGRATA program (grant agreement 813284 to S.D.), by the Italian Ministry of Health (GR-2016-02364298, to T.V.), by the Ministry of Education, University and Research-MIUR "Progetto Strategico di Eccellenza Dipartimentale" (D15D18000410001) (to S.D. as part of the Department of Medical Sciences, University of Turin). The authors thank the Nikon Imaging Facility at King's College London.

Abstract

T-cell immunoreceptor with Ig and ITIM domains (TIGIT) is an inhibitory checkpoint receptor that negatively regulates T cell responses. CD226 competes with TIGIT for binding to the CD155 ligand, delivering a positive signal to the T cell.

Here we studied expression of TIGIT and CD226 in a cohort of 115 chronic lymphocytic leukemia (CLL) patients and report expression of TIGIT and CD226 by leukemic cells. By devising a TIGIT/CD226 ratio, we showed that CLL cells favoring TIGIT over CD226 are typical of a more indolent disease, while those favoring CD226 are characterized by a shorter time-to-first-treatment and shorter progression-fee survival after first treatment. TIGIT expression was inversely correlated to the B cell receptor (BCR) signaling capacity, as determined by studying BTK phosphorylation, cell proliferation and IL-10 production. In CLL cells treated with ibrutinib, where surface IgM and BCR signaling capacity are temporarily increased, TIGIT expression was downmodulated, in line with data indicating transient recovery from anergy. Lastly, cells from Richter syndrome patients were characterized by high levels of CD226, with low to undetectable TIGIT, in keeping with their high proliferative drive.

Together, these data suggest that TIGIT contributes to CLL anergy by downregulating BCR signaling, identifying novel and actionable molecular circuits regulating anergy and modulating CLL cell functions.

Introduction

Chronic lymphocytic leukemia (CLL) is a B cell malignancy characterized by clinical and molecular heterogeneity[1]. The leukemic niche is critical to CLL development and progression in that it provides signals that influence CLL cell behavior[2, 3], among which those channeled through the B cell receptor (BCR) regulate key biological programs such as proliferation, metabolic adaptation and chemokine/cytokine secretion[4]. BCR signaling capacity varies according to somatic hypermutation of the variable region of the immunoglobulin heavy chain region (*IGHV*). CLL samples harboring unmutated (UM) *IGHV* have stronger signaling capacity compared to mutated (M) cases that display a more anergic phenotype[5].

CLL typically shows remarkable perturbations of both the innate and the adaptive immune response, which are already evident from early stages of the disease and become severe in advanced/relapsed or therapy-resistant cases[6-10]. Notably, leukemic cells play a pivotal role in shaping the microenvironment towards tolerance through multiple mechanisms[11]. For example, circulating CLL cells share phenotypic features of regulatory B-cells (Bregs) and secrete IL-10, which in turn affects T cell responses[12]. Interestingly, it was observed that IL-10 production is enhanced in anergic *IGHV*-M CLLs compared to *IGHV*-UM cases, which are characterized by a more aggressive clinical course[13].

The hypothesis behind this work is that the immunomodulatory molecule T cell immunoreceptor with Ig and ITIM domains (TIGIT) can contribute to promote B cell anergy and to shape the environment towards tolerance. TIGIT is an inhibitory receptor expressed on T, NK and NKT cells, sharing structural and mechanistic similarities with PD-1 and CTLA-4[14]. The cytoplasmic tail contains an immunoglobulin tail tyrosine (ITT)-like phosphorylation motif and an ITIM domain, like PD-1, through which TIGIT recruits the phosphatase SHIP1 to inhibit downstream activation of NF-κB, PI3K and MAPK pathways[15]. TIGIT has a competing receptor, CD226/DNAM-1 (DNAX Accessory Molecule-1), resulting in opposite signaling outcomes upon binding to the same set of ligands, similar to what described for the CTLA-4/CD28 pair[16]. The TIGIT/CD226 ligands belong to the nectin-family member poliovirus receptor (PVR), the best known of which is CD155. Signaling triggered upon CD155 binding to CD226 potentiates T cell receptor (TCR) signaling and $CD8^+$ T cell cytotoxicity against

tumor cells (positive signaling)[17]. On the contrary, concomitant TIGIT expression on the cell surface prevents CD226 activation either by sequestering CD155 or by impeding CD226 homodimerization and phosphorylation, resulting in negative signaling[18]. Whether TIGIT triggers a full inhibitory cascade or functions by preventing the CD226-mediated positive co-stimulatory signal remains unclear. Since the two receptors are co-expressed on the cell surface, a TIGIT/CD226 ratio is often preferred to highlight the imbalance towards a positive or a negative signaling outcome[19]. Even though few data are available regarding TIGIT expression in the B cell compartment, a recent paper identifies the molecule on the surface of normal human memory B cells, where it directly suppresses T cell responses[20].

In CLL patients, TIGIT expression was shown to be progressively increased in the $CD4^+$ T cell compartment, reaching the highest levels in advanced stages of the disease. Functionally, $TIGIT^+/CD4^+$ T lymphocytes sustain CLL cell viability more efficiently than the $TIGIT^-$ counterpart and TIGIT inhibition interferes with production of pro-survival cytokines by $CD4^+$ T cells[21]. On the contrary, no information is available on TIGIT expression in the leukemic cell compartment. The present study was undertaken to investigate expression of TIGIT/CD226/CD155 axis in CLL, with a specific focus on leukemic B cells, and to explore its role in BCR activation.

Methods

Sample cohort

Peripheral blood samples from CLL patients were obtained after informed consent, in accordance with Institutional Guidelines and the Declaration of Helsinki. The study was approved by the IRB of each recruiting center. We examined a retrospective cohort of 115 CLL samples and 11 buffy coats from age- and sex-matched healthy subjects. Patients' characteristics are summarized in Supplemental Table 1. Serial samples collected before treatment initiation and after 2 and 24 weeks of ibrutinib treatment were obtained from 14 additional patients (Supplemental Table 2). Clinical and molecular characteristics of CLL samples used in histologic studies on LN biopsy are reported in Supplemental Table 3.

RS patient derived xenografts (PDXs) were obtained as described[22, 23].

Where indicated, primary CLL cells were cultured in RPMI 10% FCS in the presence or absence of ibrutinib used at 1 and 5 μM for 48 hours.

Antibodies and reagents

A list of the antibodies used in Flow Cytometry and of the specific reagents used in functional assays is provided in Supplemental Table 4.

Flow Cytometry

Surface expression of TIGIT, CD226 and CD155 was evaluated by flow cytometry on CLL PBMC performing a multiparametric staining to identify B or T lymphocytes and monocytes (Supplemental Table 5). Samples were acquired with FACSCelesta cytometer (BD Biosciences) and data analyzed with FlowJo v10 Software (FlowJo,).

Modulation of TIGIT/CD226/CD155 axis

Modulation of the signaling triggered by CD155 binding either TIGIT or CD226 was performed both in the short term, to evaluate its inference on αIgM-mediated pBTK induction, and in the long term, to investigate the impact on CpG/IL-15-induced CLL proliferation. In short-term experiments, cells were pre-treated in ice for 1 hour with 5 μg/ml rhTIGIT-Fc or with αTIGIT or αCD226 blocking monoclonal antibodies (5 μg/10^6 cells) for 30

minutes followed by 1 hour with rhCD155-Fc (5 µg/ml), before αIgM stimulation. In long-term experiments, to prevent internalization, αTIGIT and αCD226 blocking monoclonal antibodies were coated onto magnetic beads and rhTIGIT-Fc and rhCD155-Fc chimeras were immobilized onto a cell culture plate. Briefly, $10x10^6$ Dynabeads Sheep anti-Mouse IgG (Invitrogen, Thermofisher) were washed twice with PBS 0.1% BSA and then coated with 1.5µg of either antibody, by incubating over night at 4 °C on a rotating wheel, following manufacturer's instructions. Coated beads were used to treat CLL cells by pre-mixing them at a 2:1 bead:cell ratio right before plating the cells in a 96-well plate. In parallel, 96-well plates were coated over night at 4 °C with 1µg/well of rhTIGIT-Fc or rhCD155-Fc chimeras.

Statistical analyses

Statistical analyses were performed with GraphPad v7 (GraphPad Software Inc, La Jolla, CA, USA). Mann-Whitney or Wilcoxon matched-pairs signed rank test were used to determine statistical significance. Contingency tests were performing using Fisher's test.

Methods for RNA extraction and qRT-PCR, Confocal microscopy, Phosflow assay, CpG/IL-15 stimulation and IL-10 production are entirely described in SI

Results

TIGIT axis expression in PBMC from CLL patients

PBMC preparations from 115 patients with a confirmed diagnosis of CLL (Supplemental Table 1) were tested for expression of TIGIT, CD226 and of the CD155 ligand and compared to a small cohort (n=11) of sex-matched healthy subjects of a comparable age. To this aim, we set-up a multiparametric staining protocol for flow cytometry to simultaneously analyze expression of the three molecules on B and T lymphocytes and monocytes (Supplemental Table 5 and Supplemental Figures 1 and 2).

Leukemic B lymphocytes variably expressed TIGIT on the cell surface, compared to normal $CD19^+$ B cells, which were uniformly negative (mean levels of expression were 21.22±21.97% of $TIGIT^+$ cells in CLL samples *vs.* 0.97±0.47% in healthy subjects). CD226 was also expressed at significantly higher levels, compared to normal B cells (mean 24±12.9% in CLL vs. 15.6±5.2% in HD) (Figure 1A).

Histologic analyses of lymph nodes (LN) confirmed low germinal center B cell-associated TIGIT expression in reactive LN samples, while CLL LNs showed higher expression levels. Similar results were obtained when examining the co-staining of CD226 with $CD20^+$ B cells (Figure 1B).

To complete the picture, we evaluated TIGIT axis expression on T lymphocytes and monocytes from CLL patients. Results indicate that i) TIGIT was variably expressed on $CD4^+$ T lymphocytes with a significant increase in advanced stages (RAI II-IV) and *IGHV*-UM CLL, in line with previous data[21]. In addition, ii) $CD8^+$ T cells were highly $TIGIT^+$, marking an exhausted phenotype (Supplemental Figure 3A and Supplemental Figure 4A). Accordingly, iii) CD226 expression on $CD8^+$ T lymphocytes decreased with advanced CLL stages, concurrent to the acquisition of further exhaustion (Supplemental Figure 3B and Supplemental Figure 4B). Lastly, iv) monocytes showed the highest CD155 levels, suggesting that this cell lineage provides the ligand to engage either TIGIT or CD226. In line with a picture of progressive immune cell dysfunction, CD155 expression on monocytes decreased in RAI II-IV CLL patients (Supplemental Figure 3C and Supplemental Figure 5A-C).

We then correlated TIGIT expression on leukemic B cells with clinical and molecular features of the disease. We found that samples bearing markers of indolent disease or good prognosis [including RAI 0-I, normal karyotype

or deletion 13 and *IGHV*-M genes] expressed TIGIT at significantly higher levels than the counterpart [RAI II-IV, trisomy 12 or deletion 11 or deletion 17, and *IGHV*-UM genes] (Figure 1C). Lower TIGIT levels were also observed in *NOTCH1* mutated cases, although this finding did not reach statistical significance. No differences could be observed according to CD38 or CD49d levels (Supplemental Figure 6A).

CD226 had an opposite trend of expression, being associated with features of a more aggressive disease behavior, such as absence of somatic hypermutations in the *IGHV* genes, presence of *NOTCH1* mutation and surface expression of CD38 and CD49, suggesting higher CD226 expression in CLL subsets that have a greater BCR signaling capacity compared to the counterparts (Figure 1C and Supplemental Figure 6A).

CD155 was generally present at low levels in CLL cells, without significant differences across disease subsets (Supplemental Figure 7).

Definition of an operational TIGIT:CD226 ratio

Considering that TIGIT and CD226 have opposing roles on the cell surface and compete for the binding to the same ligand, we determined a TIGIT:CD226 ratio, based on percentage of expression. A TIGIT:CD226 ratio ≥1 indicates a prevalence of TIGIT expressing cells and consequently a predominance of negative signaling, whereas a TIGIT:CD226 ratio <1 indicates the prevalence of CD226 expressing cells and therefore a positive signaling. In line with this reasoning, CLL samples with a TIGIT:CD226 ratio ≥1 were enriched in the good prognosis subsets, while samples with ratio <1 were more frequent in the presence of adverse prognostic markers (e.g., advanced stages, *IGHV*-UM, unfavorable cytogenetics, *NOTCH1* mutations), confirming the validity of this approach (Figure 2A and Supplemental Figure 6B).

Interestingly, prevalence of CD226 signaling, as defined by TIGIT:CD226 ratio <1, correlates with significantly earlier time to first treatment and shorter progression-free survival after first line therapy (Figure 2B).

TIGIT expression is associated with CLL anergy

To investigate the interplay between TIGIT and the BCR signaling capacity, we selected a homogeneous subset of samples carrying *IGHV*-UM, normal FISH profile or deletion 13q as sole abnormality and without *NOTCH1* mutation, to avoid experimental biases[24]. We found an inverse correlation between TIGIT expression and BCR

signaling capacity, evaluated analyzing baseline surface IgM levels and BTK phosphorylation in response to IgM crosslinking as read outs (Figure 3A, left panels). Moreover, when splitting CLL samples according to TIGIT:CD226 ratio, we confirmed that samples with ratio<1 ($TIGIT^-$) had significantly higher surface IgM levels and stronger phospho-BTK induction than cases with ratio ≥1 ($TIGIT^+$) (Figure 3A, right panels).

We next examined whether high TIGIT levels were associated with weaker responses of CLL cells to activation/proliferation signals, such as CpG/IL-15, analyzed in the same CLL subset used to test BCR signaling. In line with the results obtained for the BCR signaling studies, when dividing samples according to the TIGIT:CD226 ratio, samples with prevalence of TIGIT showed a lower proliferative response to CpG/IL-15 compared to samples with a <1 ratio (Figure 3B, upper panel).

Analysis of TIGIT and CD226 expression in these cells, after 6 days exposure to CpG/IL-15, showed a marked up-regulation of CD226, with a concomitant slight TIGIT down-modulation (Supplemental Figure 8A). Unstimulated cells showed a high level of spontaneous apoptosis; in the remaining live cells, CD226 expression was downregulated compared to the expression levels before starting *in vitro* culture (Figure 3B, lower panel). Modulation of CD226 and TIGIT levels could explain, at least in part, the observation that $TIGIT^+$ CLL samples showed a productive proliferative response, albeit weaker than $TIGIT^-$ samples. Accordingly, the TIGIT:CD226 ratio in stimulated cells was <1 in all samples, in line with a prevalence of "positive" signaling (Supplemental Figure 8B).

In line with these findings, we identified that CLL LN biopsies with higher TIGIT expression showed lower CD226 levels (Figure 3C). These tissues samples had a significantly lower expression of the proliferation marker Ki67, when compared to samples showing low TIGIT and high CD226. Consistently, we found that $CD226^+$ CLL cells were mainly associated with Ki67 expression regardless of TIGIT levels, that was significant in $TIGIT^{low}$, $CD226^{high}$ LNs cases as revealed by Ki67/TIGIT versus Ki67/CD226 colocalization image analysis (Figure 3C).

$TIGIT^+$ CLL cells produce more IL-10

Considering that *IGHV*-M anergic CLL cells produce and secrete more IL-10 than *IGHV*-UM reactive cells[13], we investigated whether high TIGIT expression correlated with IL-10 production. We found that samples harboring

TIGIT:CD226 ratio ≥1 had significantly higher *IL10* mRNA levels, both in the *IGHV*-UM and the *IGHV*-M CLL groups (Figure 4A). Similar results were obtained when measuring IL-10 production by flow cytometry, where $TIGIT^+$ CLL cells stained more positive for IL-10 than $TIGIT^-$ cells after 5 hours stimulation with phorbol 12-myristate 13-acetate (PMA) and ionomycin, even in *IGHV*-UM cases (Figure 4B-C). The observation that *IGHV*-M cells showed higher *IL10* expression and production, at the mRNA and at the protein levels, respectively, both in the $TIGIT^+$ and in the $TIGIT^-$ subsets, suggests that TIGIT is associated with different IL-10 profiles but also that other regulatory mechanisms exist.

TIGIT axis expression during disease follow up

We next studied modulation of surface TIGIT, CD226 and CD155 over time, focusing specifically on the effects exerted by BTK inhibitors, since they are known to modulate BCR signaling. To this aim, we took advantage of a cohort of 14 samples collected systematically before ibrutinib initiation, after 2 weeks and after 24 weeks of treatment. Characterization of samples is reported in Supplemental Table 2. Previous studies have shown that btk blockade is followed by up-regulation of surface IgM levels, evident already after 1 week on therapy and maintained for at least 3 months[25]. This apparently paradoxical behavior was observed also in our cohort, where sIgM levels were increased after 2 weeks of treatment and remained higher than the baseline at 24 weeks (Figure 5A). In line with heightened BCR signaling activity, surface TIGIT, which was expressed before therapy initiation by all samples, invariably decreased upon ibrutinib treatment, starting within the first 2 weeks of treatment and reaching minimal levels at the 24-week timepoint (Figure 5B). TIGIT mRNA levels showed the same behavior (Supplemental Figure 9A). On the contrary, mRNA levels of CD226 showed a marked increase (Supplemental Figure 9A), while surface levels were minimally, but significantly decreased (Figure 5C, left panel), raising question on whether the molecule can reach the cell surface. However, given the relative changes of TIGIT and CD226, their ratio dropped to <1 in all samples examined, including those having a ratio ≥1 before treatment, suggesting a switch towards a "positive" CD226-mediated signaling (Figure 5C, right panel). TIGIT down-regulation appeared specific of B cells, as we found that ibrutinib treatment did not

alter its expression on $CD4^+$ or $CD8^+$ T cell subsets (Supplemental Figure 9C-D). In contrast, CD155 expression showed minimal decrease in surface expression across patients' follow up (Supplemental Figure 9B).

This response to ibrutinib was documented also in vitro, by exposing primary CLL cells from untreated patients to ibrutinib (1 μM and 5 μM for 48 hours). In these cells, we observed increased sIgM levels, with a concomitant decrease of the TIGIT:CD226 ratio (Figure 5D and Supplemental Figure 9E). Previous investigators have reported that upon btk inhibition, the BCR retains the capability to mobilize Ca^{2+} in response to antibody ligation, as well as the capability of tyrosine phosphorylating syk and ERK1/2[26]. In our samples, despite inhibition of tyrosine phosphorylation of btk, a marked increase in intracellular Ca^{2+} mobilization upon BCR ligation was observed, comparing untreated vs ibrutinib-treated primary CLL cells. The same cells showed prominent tyrosine phosphorylation of syk and ERK1/2, clearly indicating that the BCR pathway is bypassing the signaling block imposed by ibrutinib. (Figure 5E).

TIGIT and CD226 are expressed on Richter's Syndrome samples

Stemming from these observations, we evaluated expression of TIGIT and CD226 in cases of Richter's Syndrome (RS), a rare but often fatal complication of CLL characterized by transformation of the leukemia into an aggressive lymphoma[27-29]. To this aim, we exploited RNAseq analysis performed on primary FFPE RS lymph nodes and compared it to that of CLL samples and matched healthy subjects, from previously published datasets [EGA accession numbers EGAD00001004046 and EGAD00001000258[30, 31]]. RS samples showed lower TIGIT expression compared to CLL samples, in line with our observation of TIGIT marking a more indolent disease. Accordingly, CD226 expression in RS cell was the highest compared to HD and CLL samples (Figure 6A). Results were substantiated by using RS-patient derived xenograft models recently established in our lab[22, 23]. Both qPCR performed on 4 RS-PDXs at different passages and flow cytometry analyses confirmed the RNAseq results, with TIGIT being expressed at lower levels compared to CLL cases and CD226 showing the highest expression (Figure 6B-C). Interestingly, all these four models show highly active BCR signaling pathway[32].

CD155 transcript levels were barely detectable in RS samples, although the molecule was expressed on the cell surface (Supplemental Figure 10).

Modulation of TIGIT and CD226 signaling

To understand the functional role of TIGIT and CD226 in altering BCR signaling capacity and cell proliferation, we selectively interfered with either receptor/ligand interaction, taking advantage of specific recombinant human (rh) Fc chimeras or blocking monoclonal antibodies. Read-outs were BTK phosphorylation in response to αIgM-mediated BCR crosslinking or Ki67 staining following CpG/IL-15 culture, respectively. A schematic representation of the experiments and reagents is depicted in Figure 7A. Specifically, we used: i) a rhTIGIT-Fc chimera that sequesters CD155 expressed on the cell surface and prevents it from binding either TIGIT or CD226, blocking downstream signaling of the prevalent receptor in that CLL population; ii) a rhCD155-Fc chimera that works as an artificial ligand and can bind and activate both TIGIT and CD226, depending on which receptor is prevalent. To discriminate between the activation of one receptor and the other, we used the rhCD155-Fc chimera in combination with iii) blocking monoclonal antibodies directed against either TIGIT or CD226 (αTIGIT or αCD226).

Experiments were carried out in the same *IGHV*-UM CLL cases with normal FISH profile or deletion 13 used in previous experiments. Pre-treatment of $TIGIT^-$ CLL cells with rhTIGIT-Fc affects mostly CD226 signaling, which is more expressed than TIGIT in these samples. We found that the BCR signaling capacity upon receptor engagement in the presence of rhTIGIT-Fc was significantly downregulated in $TIGIT^-$ samples compared to αIgM given alone, and phospho-BTK induction was similar to that of $TIGIT^+$ samples. In contrast, pre-treatment of $TIGIT^+$ CLL cells with rhTIGIT-Fc mostly prevents CD155 binding to TIGIT, likely abrogating its negative regulation of the BCR. Accordingly, in these samples, αIgM-induced BTK phosphorylation was significantly increased in the presence of rhTIGIT-Fc, and was more similar to that of $TIGIT^-$ samples. Furthermore, stimulation of the BCR in the presence of rhCD155-Fc and of αTIGIT blocking antibody enhanced BTK phosphorylation in $TIGIT^+$ samples, while this combination had no effects on $TIGIT^-$ samples, that already had maximal phospho-BTK induction. Lastly, pre-treatment of CLL cells with rhCD155-Fc and of αCD226 blocking antibody downmodulated BCR signaling capacity of $TIGIT^-$ samples, where CD226 is prevalent and could help improving BCR responses, to

levels comparable to those of TIGIT^{+} CLLs, whose phospho-BTK induction was unaffected in the presence of agents preventing CD226 signaling (Figure 7B).

Similar results were obtained when examining the proliferative response to CpG/IL-15 stimulation in the same conditions (Figure 7C).

These results suggest that CD155 binding to TIGIT triggers an inhibitory signaling that decreases responsiveness of CLL cells to the antigen, and that, if we interrupt CD155-TIGIT interactions we can boost CLL cell responses. On the other hand, CD155 binding to CD226 exerts an opposite “positive” effect on intracellular signaling and interrupting this axis might induce CLL cell anergy.

Discussion

This work shows that the immunomodulatory molecule TIGIT is expressed by CLL cells where it is a marker of anergy. TIGIT was identified nearly a decade ago and shown to be part of an axis including also CD226 and CD155 that shares similarities with other checkpoint inhibitors[33]. In the current view, TIGIT and CD226 are expressed by T cells and can negatively (TIGIT) or positively (CD226) impact on TCR signaling, once engaged by the common CD155 ligand. Coherent with this view, T cells expressing high levels of TIGIT are reported in different cancers where they define a subset of exhausted and dysfunctional T lymphocytes[21, 34-36]. In CLL, high TIGIT expression is found on T lymphocytes from patients with advanced disease, co-expressing exhaustion markers [[21] and Supplementary Figure 6].

The recent finding of TIGIT expression on normal memory B cells, where it directly contributes to suppress T cell responses[20], prompted us to extend these observations to CLL cells. Here, we show for the first time that circulating and residential leukemic B cells express TIGIT and CD226, at variance with the normal $CD19^+$ subset. CD155, in contrast, was mostly expressed on the monocyte compartment. When dividing our cohort of 115 patients according to specific prognostic markers, we observed that high TIGIT was associated with features of indolent disease while high CD226 was more frequent in subsets characterized by elevated BCR signaling capacity (e.g., *IGHV*-UM, *NOTCH1*-M or $CD38^+$ and $CD49d^+$ cases). Since TIGIT and CD226 are concomitantly present on the cell surface, we devised a ratio between the two markers: a ratio ≥1 indicates predominance of TIGIT and hence of inhibitory effects (negative signaling), while a ratio in favor of CD226 prompts for a co-stimulatory effect (positive signaling). Accordingly, aggressive CLLs were enriched with samples showing a ratio in favor of CD226. It is therefore likely that this axis might modulate signaling of CLL cells, similar to what observed in T lymphocytes.

To determine a possible role for TIGIT in CLL homeostasis, we first explored the effects on BCR signaling capacity, specifically focusing on *IGHV*-UM samples, selected to harbor high or low surface TIGIT. We found an inverse correlation between TIGIT expression and baseline sIgM levels or the induction of BTK phosphorylation in response to receptor engagement, suggesting that surface TIGIT is associated with a more anergic CLL

behavior. In a cohort of samples collected systematically after ibrutinib therapy, we observed a sharp decrease in surface TIGIT following treatment. This is in line with the recent observation that leukemic cells, released from the LN by ibrutinib, upregulate sIgM and SYK because they no longer receive persistent antigen stimulation, as if they turned less anergic despite downstream inhibition of BTK[25]. The mechanism behind TIGIT downregulation remains to be determined. Speculatively, it could rely on the inhibition of transcription factors downstream to the BCR signaling, including NFATC1[37], FOXP1[38] and NFKB[39] that have putative binding sites on TIGIT promoter [not shown, prediction made using CiiiDER online tool at http://www.ciiider.org/ and[40]].

TIGIT downregulation with concomitant surface IgM upregulation were also confirmed by *in vitro* exposure of primary CLL cells to ibrutinib. While btk tyrosine phosphorylation was invariably inhibited in these cells, BCR ligation was followed by syk and ERK1/2 tyrosine phosphorylation and mobilization of intracellular Ca^{2+} to levels higher than those observed in untreated cells, indicating recovery from anergy. This behavior was previously attributed to the interruption of chronic antigen stimulation due to release of CLL cells exposed to ibrutinib from the lymph node niche, at the same time making them more dependent on BCR engagement and consequently more susceptible to apoptosis if the ligand is not present, as is the case for peripheral circulation[25].

A formal demonstration of the effects of TIGIT and CD226 on BCR signaling capacity comes from experiments where interactions of these receptors with the CD155 ligand were interrupted using specific recombinant chimeras and monoclonal antibodies. rhTIGIT-Fc chimera sequesters CD155 and prevents its binding to either receptor, thus affecting the signaling through the prevalent receptor on the cell surface (Figure 7Aii). Therefore, in $TIGIT^-$ samples, blocking CD155 affects mostly signaling through CD226, removing its positive contribution to the BCR signaling and, consistently, we observed a reduced αIgM-induced BTK phosphorylation. In contrast, in $TIGIT^+$ samples, TIGIT signaling is affected by CD155 sequestering, removing its inhibitory effect and increasing BTK phosphorylation. Comparable results were achieved when selectively activating CD226 or TIGIT by providing chimeric CD155 ligand together with a monoclonal antibody blocking the unintended receptor (Figure 7Aiii-iv). Using the same experimental asset, we examined CLL cell proliferation in response to

CpG/IL-15 stimulation and observed significant differences between TIGIT$^+$ and TIGIT$^-$ samples, with the latter showing a proliferative advantage over the former. Again, when interrupting TIGIT/CD226 interactions with CD155 we could modulate responses to CpG/IL-15 with different outcomes in TIGIT$^+$ and TIGIT$^-$ samples.

Lastly, when analyzing IL-10 secretion in our sample cohort, we found that TIGIT$^+$ CLLs produce more IL-10 than the TIGIT$^-$ ones, both in the *IGHV*-M and in the *IGHV*-UM subsets. This finding is in line with previous observations that TIGIT$^+$ normal memory B cells suppress T cell responses more efficiently than the TIGIT$^-$ counterpart, possibly via IL-10[20], and also with existing literature showing that IL-10 production is enhanced in more anergic CLLs and associated with less aggressive clinical phenotype[13, 41].

Our results indicate that TIGIT and CD226 are aberrantly expressed on leukemic B cells, and this is the first time that deregulation of this axis is described on tumor cells and not only in the T cell compartment. In addition, this work provides evidence of an association between TIGIT expression and an anergic phenotype of the CLL cell. The mechanism behind TIGIT upregulation in CLL is still not understood. However, a recent paper reported a signature of aberrantly expressed immune regulatory molecules, including TIGIT, in CLL cells with a peculiar methylation pattern compared to healthy B lymphocytes[42].

The translational implications of these results remain to be determined. Since therapeutic anti-TIGIT antibodies are in clinical trials for cancer patients, it would be tempting to determine whether in CLL patients that may revert anergy, increasing BCR signaling capacity, and therefore making leukemic cells more susceptible to targeted inhibitors. Further research will tell us more about this immunoregulatory pathway and its possible clinical implications.

References

1. Chiorazzi N, Rai KR, Ferrarini M. Chronic lymphocytic leukemia. N Engl J Med. 2005;352(8):804-815.
2. Puente XS, Jares P, Campo E. Chronic lymphocytic leukemia and mantle cell lymphoma: crossroads of genetic and microenvironment interactions. Blood. 2018;131(21):2283-2296.
3. Herishanu Y, Perez-Galan P, Liu D, et al. The lymph node microenvironment promotes B-cell receptor signaling, NF-kappaB activation, and tumor proliferation in chronic lymphocytic leukemia. Blood. 2011;117(2):563-574.
4. Stevenson FK, Krysov S, Davies AJ, Steele AJ, Packham G. B-cell receptor signaling in chronic lymphocytic leukemia. Blood. 2011;118(16):4313-4320.
5. Packham G, Krysov S, Allen A, et al. The outcome of B-cell receptor signaling in chronic lymphocytic leukemia: proliferation or anergy. Haematologica. 2014;99(7):1138-1148.
6. Forconi F, Moss P. Perturbation of the normal immune system in patients with CLL. Blood. 2015;126(5):573-581.
7. Peters FS, Strefford JC, Eldering E, Kater AP. T-cell dysfunction in chronic lymphocytic leukemia from an epigenetic perspective. Haematologica. 2021;106(5):1234-1243.
8. Vlachonikola E, Stamatopoulos K, Chatzidimitriou A. T Cells in Chronic Lymphocytic Leukemia: A Two-Edged Sword. Front Immunol. 2020;11:612244.
9. Fiorcari S, Maffei R, Atene CG, Potenza L, Luppi M, Marasca R. Nurse-Like Cells and Chronic Lymphocytic Leukemia B Cells: A Mutualistic Crosstalk inside Tissue Microenvironments. Cells. 2021;10(2):217.
10. Griggio V, Perutelli F, Salvetti C, et al. Immune Dysfunctions and Immune-Based Therapeutic Interventions in Chronic Lymphocytic Leukemia. Front Immunol. 2020;11:594556.
11. Arruga F, Gyau BB, Iannello A, Vitale N, Vaisitti T, Deaglio S. Immune Response Dysfunction in Chronic Lymphocytic Leukemia: Dissecting Molecular Mechanisms and Microenvironmental Conditions. Int J Mol Sci. 2020;21(5):1825.
12. DiLillo DJ, Weinberg JB, Yoshizaki A, et al. Chronic lymphocytic leukemia and regulatory B cells share IL-10 competence and immunosuppressive function. Leukemia. 2013;27(1):170-182.
13. Drennan S, D'Avola A, Gao Y, et al. IL-10 production by CLL cells is enhanced in the anergic IGHV mutated subset and associates with reduced DNA methylation of the IL10 locus. Leukemia. 2017;31(8):1686-1694.
14. Yu X, Harden K, Gonzalez LC, et al. The surface protein TIGIT suppresses T cell activation by promoting the generation of mature immunoregulatory dendritic cells. Nat Immunol. 2009;10(1):48-57.
15. Liu S, Zhang H, Li M, et al. Recruitment of Grb2 and SHIP1 by the ITT-like motif of TIGIT suppresses granule polarization and cytotoxicity of NK cells. Cell Death Differ. 2013;20(3):456-464.
16. Le Mercier I, Lines JL, Noelle RJ. Beyond CTLA-4 and PD-1, the Generation Z of Negative Checkpoint Regulators. Front Immunol. 2015;6:418.
17. Chan CJ, Andrews DM, McLaughlin NM, et al. DNAM-1/CD155 interactions promote cytokine and NK cell-mediated suppression of poorly immunogenic melanoma metastases. J Immunol. 2010;184(2):902-911.
18. Johnston RJ, Comps-Agrar L, Hackney J, et al. The immunoreceptor TIGIT regulates antitumor and antiviral CD8(+) T cell effector function. Cancer Cell. 2014;26(6):923-937.
19. Deng C, Li W, Fei Y, et al. Imbalance of the CD226/TIGIT Immune Checkpoint Is Involved in the Pathogenesis of Primary Biliary Cholangitis. Front Immunol. 2020;11:1619.
20. Hasan MM, Nair SS, O'Leary JG, et al. Implication of TIGIT(+) human memory B cells in immune regulation. Nat Commun. 2021;12(1):1534.
21. Catakovic K, Gassner FJ, Ratswohl C, et al. TIGIT expressing CD4+T cells represent a tumor-supportive T cell subset in chronic lymphocytic leukemia. Oncoimmunology. 2017;7(1):e1371399.
22. Vaisitti T, Braggio E, Allan JN, et al. Novel Richter Syndrome Xenograft Models to Study Genetic Architecture, Biology, and Therapy Responses. Cancer Res. 2018;78(13):3413-3420.

23. Vaisitti T, Arruga F, Vitale N, et al. ROR1 targeting with the antibody-drug conjugate VLS-101 is effective in Richter syndrome patient-derived xenograft mouse models. Blood. 2021;137(24):3365-3377.
24. Arruga F, Bracciama V, Vitale N, et al. Bidirectional linkage between the B-cell receptor and NOTCH1 in chronic lymphocytic leukemia and in Richter's syndrome: therapeutic implications. Leukemia. 2020;34(2):462-477.
25. Drennan S, Chiodin G, D'Avola A, et al. Ibrutinib Therapy Releases Leukemic Surface IgM from Antigen Drive in Chronic Lymphocytic Leukemia Patients. Clin Cancer Res. 2019;25(8):2503-2512.
26. Chiodin G, Drennan S, Martino EA, et al. High surface IgM levels associate with shorter response to ibrutinib and BTK bypass in patients with CLL. Blood Adv. 2022;6(18):5494-5504.
27. Tadmor T, Levy I. Richter Transformation in Chronic Lymphocytic Leukemia: Update in the Era of Novel Agents. Cancers (Basel). 2021;13(20):5141.
28. Condoluci A, Rossi D. Richter Syndrome. Curr Oncol Rep. 2021;23(3):26.
29. Rossi D, Spina V, Gaidano G. Biology and treatment of Richter syndrome. Blood. 2018;131(25):2761-2772.
30. Beekman R, Chapaprieta V, Russinol N, et al. The reference epigenome and regulatory chromatin landscape of chronic lymphocytic leukemia. Nat Med. 2018;24(6):868-880.
31. Ferreira PG, Jares P, Rico D, et al. Transcriptome characterization by RNA sequencing identifies a major molecular and clinical subdivision in chronic lymphocytic leukemia. Genome Res. 2014;24(2):212-226.
32. Iannello A, Vitale N, Coma S, et al. Synergistic efficacy of the dual PI3K-delta/gamma inhibitor duvelisib with the Bcl-2 inhibitor venetoclax in Richter syndrome PDX models. Blood. 2021;137(24):3378-3389.
33. Ge Z, Peppelenbosch MP, Sprengers D, Kwekkeboom J. TIGIT, the Next Step Towards Successful Combination Immune Checkpoint Therapy in Cancer. Front Immunol. 2021;12:699895.
34. Freed-Pastor WA, Lambert LJ, Ely ZA, et al. The CD155/TIGIT axis promotes and maintains immune evasion in neoantigen-expressing pancreatic cancer. Cancer Cell. 2021;39(10):1342-1360.e14.
35. Chauvin JM, Pagliano O, Fourcade J, et al. TIGIT and PD-1 impair tumor antigen-specific CD8(+) T cells in melanoma patients. J Clin Invest. 2015;125(5):2046-2058.
36. Shao Q, Wang L, Yuan M, Jin X, Chen Z, Wu C. TIGIT Induces (CD3+) T Cell Dysfunction in Colorectal Cancer by Inhibiting Glucose Metabolism. Front Immunol. 2021;12:688961.
37. Wolf C, Garding A, Filarsky K, et al. NFATC1 activation by DNA hypomethylation in chronic lymphocytic leukemia correlates with clinical staging and can be inhibited by ibrutinib. Int J Cancer. 2018;142(2):322-333.
38. Cerna K, Oppelt J, Chochola V, et al. MicroRNA miR-34a downregulates FOXP1 during DNA damage response to limit BCR signalling in chronic lymphocytic leukaemia B cells. Leukemia. 2019;33(2):403-414.
39. Rozovski U, Harris DM, Li P, et al. Activation of the B-cell receptor successively activates NF-kappaB and STAT3 in chronic lymphocytic leukemia cells. Int J Cancer. 2017;141(10):2076-2081.
40. Gearing LJ, Cumming HE, Chapman R, et al. CiiiDER: A tool for predicting and analysing transcription factor binding sites. PLoS One. 2019;14(9):e0215495.
41. Hanna BS, Llao-Cid L, Iskar M, et al. Interleukin-10 receptor signaling promotes the maintenance of a PD-1(int) TCF-1(+) CD8(+) T cell population that sustains anti-tumor immunity. Immunity. 2021;54(12):2825-2841.e10.
42. Wierzbinska JA, Toth R, Ishaque N, et al. Methylome-based cell-of-origin modeling (Methyl-COOM) identifies aberrant expression of immune regulatory molecules in CLL. Genome Med. 2020;12(1):29.

Figure Legends

Figure 1. TIGIT and CD226 are deregulated in CLL and differentially expressed among patient subsets. A. Percentages of TIGIT$^+$ and CD226$^+$ cells in a cohort of 115 CLL samples and 11 age- and sex-matched healthy donor (HD). Statistical analysis: Student's t-test. **B.** Representative multispectral immunofluorescence confocal images of non-malignant reactive (n=4) or CLL (n=6) lymph node formalin-fixed paraffin-embedded biopsy tissues for TIGIT or CD226 (red) expression in the lymph node microenvironment (CD20, white). RLN: Reactive lymph node; CLL LN: CLL lymph node. Original magnification, x20, scale bar: 50 μm. **C.** From left to right: percentages of TIGIT$^+$ and CD226$^+$cells in samples stratified according to RAI stage and cytogenetic profile (top panels); percentages of TIGIT$^+$ and CD226$^+$cells in samples stratified according to the *IGHV* mutational status and to the presence of *NOTCH1* mutations (bottom panels). Statistical analyses: Student's t-test.

Figure 2. Ratio between TIGIT$^+$ and CD226$^+$ cells in CLL samples. A. We calculated a ratio between the percentage of TIGIT$^+$ and CD226$^+$ cells in our cohort of CLL samples. A ratio ≥1 indicates prevalence of TIGIT$^+$ cells and predominant negative signaling; a ratio <1 indicates prevalence of CD226$^+$ cells and predominant positive signaling. For each clinical or molecular marker (RAI stage, *IGHV* mutational status, cytogenetics, *NOTCH1* mutations) there is a dot plot showing ratio values for each sample (left) and a contingency plot indicating the enrichment of samples with ratio ≥1 or <1 in either prognostic category. Dashed line at Y=1 indicates the threshold to discriminate between negative signaling (TIGIT/CD226 ratio≥1, prevalence of TIGIT) and positive signaling (TIGIT/CD226 ratio<1, prevalence of CD226). Statistical analyses: Student's t-test. **B.** Kaplan-Meier curves comparing the time to first treatment and the progression-free survival both before and after treatment of CLL patients divided according to TIGIT/CD226 ratio. Statistical analyses: Mantel-Cox test.

Figure 3. High surface TIGIT is associated with CLL cell anergy. A. Top panels. Inverse correlation between surface IgM levels and the percentage of TIGIT expressing cells in CLL samples harboring *IGHV*-UM and normal karyotype or deletion 13 as sole abnormality (left), and surface IgM levels in CLL samples divided according to

TIGIT:CD226 ratio (right). Bottom panels. Inverse correlation between the induction of BTK phosphorylation (pBTK) upon BCR stimulation and the TIGIT:CD226 ratio in CLL samples (left), and fold changes (FC) of αIgM-mediated pBTK induction in CLL samples divided according to TIGIT:CD226 ratio (right). **B.** Ki67 staining of $TIGIT^{+}$ and $TIGIT^{-}$ CLL samples (top) and flow cytometry analysis of surface CD226 upregulation (bottom) in response to CpG/IL-15 culture. **C.** Representative multispectral immunofluorescence and 3D volume rendered confocal images of $TIGIT^{high}/CD226^{low}$ (n=3) or $TIGIT^{low}/CD226^{high}$ (n=3) CLL lymph node formalin-fixed paraffin-embedded biopsy tissues stained for CD20 (blue), ki67 (magenta) and TIGIT or CD226 (green). Original magnification, x20, scale bars of the larger image: 100 µm, of the lower image: 50 µm. The images on the right represent a magnification of the top image, as indicated by the arrow. Quantification of the colocalization of Ki67 and TIGIT or Ki67 and CD226 limited to $CD20^{+}$ cells from CLL lymph node tissues. Graphs relative to the quantification in $TIGIT^{high}/CD226^{low}$ LNs (Top), $TIGIT^{low}/CD226^{high}$ LNs (middle) or all the LN samples together (bottom) are shown. Statistical analyses: Student's t-test.

Figure 4. $TIGIT^{+}$ cells produce more IL-10. A. qRT-PCR analysis of *IL10* baseline expression of CLL samples divided according to *IGHV* mutational status and TIGIT surface levels. **B.** FACS analysis of IL-10 intracellular staining after 5h stimulation with PMA (50 ng/mL) and 1µM ionomycin in CLL samples divided according to *IGHV* mutational status and TIGIT surface levels. **C.** Representative flow cytometry plots of IL-10 production in unstimulated (NS) and stimulated (PMA/Iono) CLL cells. Statistical analyses: Student's t-test.

Figure 5. TIGIT and CD226 expression during the follow up of CLL patients treated with ibrutinib. A. Surface IgM levels (MFI, Mean Fluorescence Intensity) before and during ibrutinib therapy. Surface expression of TIGIT (**B**) and CD226 (**C**, left panel) expression before treatment initiation (UnTX), after 2 and 24 weeks of ibrutinib therapy. **C.** (right panel) TIGIT:CD226 ratio at pre-treatment (PreTX) and after 2 or 24 weeks (2w and 24w) after ibrutinib initiation. Dashed line at Y=1 indicates the threshold to discriminate between negative signaling (TIGIT:CD226 ratio≥1, prevalence of TIGIT) and positive signaling (TIGIT:CD226 ratio<1, prevalence of CD226).

Statistical analyses (**A-C**): one-way Anova test. **D** (left panel) Surface IgM levels (MFI) of CLL cells treated *in vitro* with 1 and 5 μM ibrutinib for 48 hours. **D** (right panel) TIGIT:CD226 ratio measured in primary CLL cells in the presence or in the absence of ibrutinib used at 1 and 5 μM for 48 hours. The dashed line at Y=1 indicates the threshold to discriminate between negative and positive signaling. **E.** Phospho-btk MFI levels in response to anti-IgM ligation in primary CLL cells left untreated or exposed to 1 μM ibrutinib for 48 hours (left panel). In the same cells, intracellular Ca^{2+} levels were monitored by flow cytometry (middle panel) and syk and ERK1/2 phosphorylation by western blot (right panels) (**D-E**) Statistical analyses: Student's t-test.

Figure 6. TIGIT and CD226 expression in RS. A. Transcript per million (TPM) values of TIGIT and CD226 from RNAseq experiments carried out in normal B cells, CLL samples and primary FFPE-embedded LN from RS samples. **B.** qRT-PCR analysis of TIGIT and CD226 expression in our cohort of healthy subjects, CLL samples and RS-PDX models at different passages. **C.** Flow cytometry analysis of TIGIT and CD226 surface expression in HD, CLL and RS-PDXs. Statistical analyses: Student's t-test.

Figure 7. Modulation of TIGIT and CD226 interaction with CD155. A. Schematic representation of the mechanisms of action of rhTIGIT-Fc and rhCD155-Fc chimeras and of αTIGIT and αCD226 blocking monoclonal antibodies (mAb): i) CD155 can bind either TIGIT or CD226 triggering opposite signaling outcome; ii) rhTIGIT-Fc chimera prevents CD155 binding and can therefore inhibit both TIGIT and CD226 signaling, thus affecting the signaling through the prevalent receptor on the cell surface. rhCD155-Fc chimera works as an artificial ligand and can bind to either receptor, therefore iii) when giving it in combination with the αTIGIT blocking mAb it is possible to induce signaling through CD226, while iv) in combination with αCD226 mAb, signaling through TIGIT is preserved. **B.** Flow cytometry analysis of pBTK induction in response to αIgM-mediated BCR crosslink in the presence of modulators of TIGIT and CD226 activity: top panels show plots of two representative $TIGIT^+$ and $TIGIT^-$ samples, bottom panel show cumulative results of pBTK induction. **C.** Cumulative results of Ki67 staining

upon CpG/IL-15 culture in the presence of modulators of TIGIT and CD226 activity. Statistical analyses: Student's t-test.

Figure 1

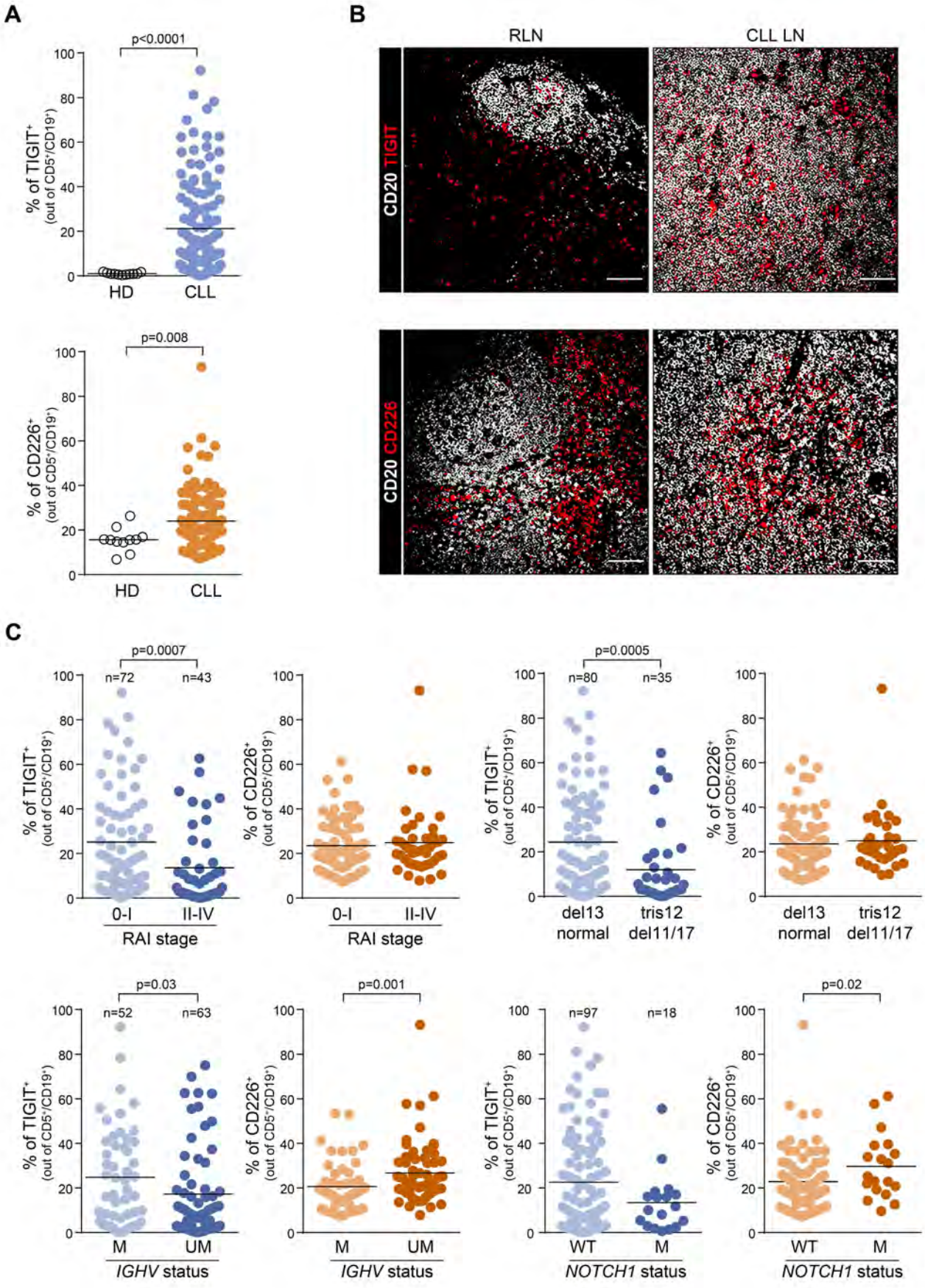
A
p<0.0001
% of TIGIT+ (out of CD5+/CD19+)
HD
CLL
p=0.008
% of CD226+ (out of CD5+/CD19+)
HD
CLL
B
RLN
CLL LN
CD20 TIGIT
CD20 CD226
C
p=0.0007
n=72
n=43
% of TIGIT+ (out of CD5+/CD19+)
0-I
II-IV
RAI stage
% of CD226+ (out of CD5+/CD19+)
0-I
II-IV
RAI stage
p=0.0005
n=80
n=35
% of TIGIT+ (out of CD5+/CD19+)
del13 normal
tris12 del11/17
% of CD226+ (out of CD5+/CD19+)
del13 normal
tris12 del11/17
p=0.03
n=52
n=63
% of TIGIT+ (out of CD5+/CD19+)
M
UM
IGHV status
p=0.001
% of CD226+ (out of CD5+/CD19+)
M
UM
IGHV status
n=97
n=18
% of TIGIT+ (out of CD5+/CD19+)
WT
M
NOTCH1 status
p=0.02
% of CD226+ (out of CD5+/CD19+)
WT
M
NOTCH1 status

Figure 2

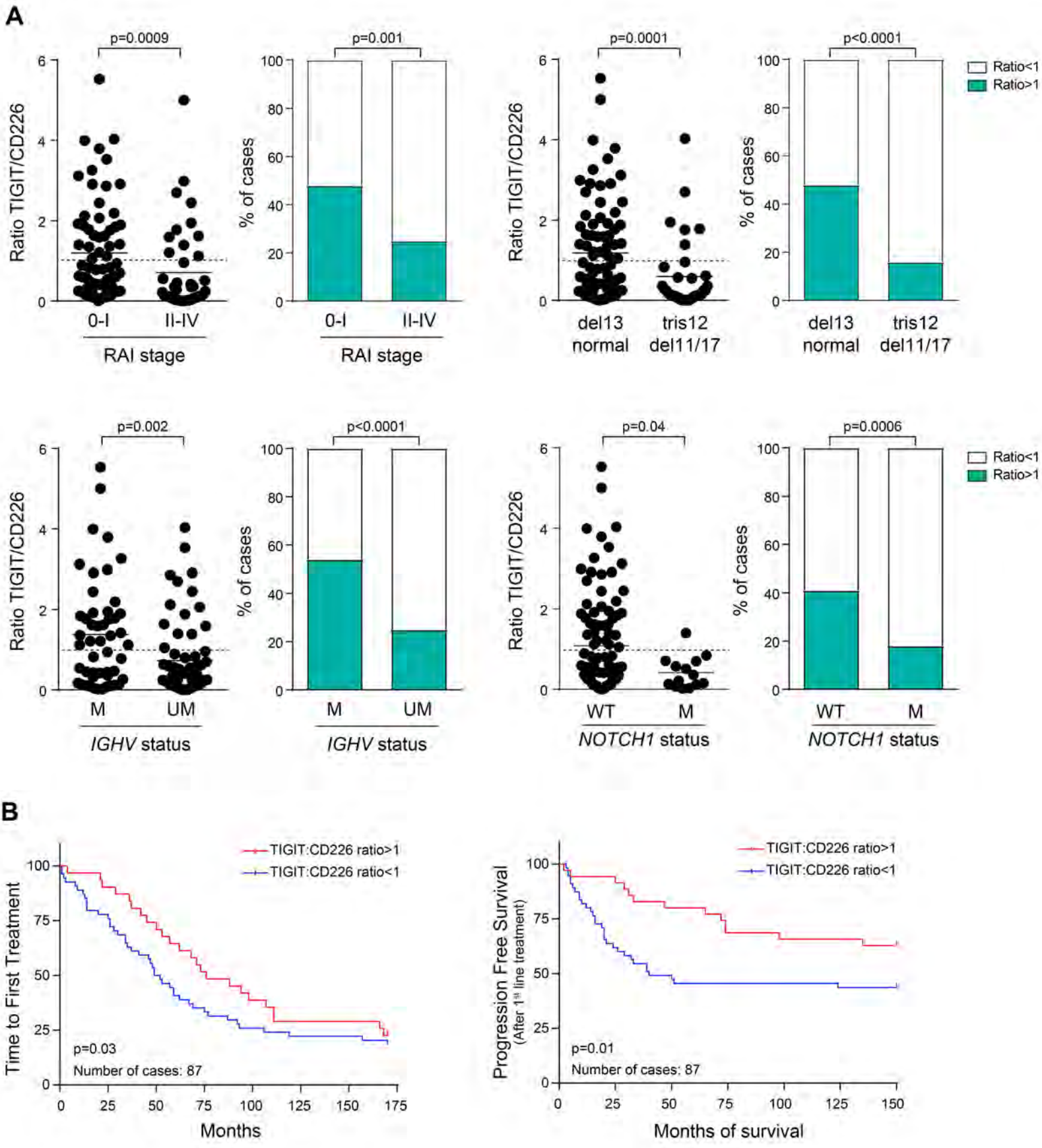
A
p=0.0009
Ratio TIGIT/CD226
0-I
II-IV
RAI stage
p=0.001
% of cases
Ratio<1
Ratio>1
p=0.0001
del13 normal
tris12 del11/17
p<0.0001
p=0.002
M
UM
IGHV status
p<0.0001
p=0.04
WT
M
NOTCH1 status
p=0.0006
B
TIGIT:CD226 ratio>1
TIGIT:CD226 ratio<1
Time to First Treatment
p=0.03
Number of cases: 87
Months
Progression Free Survival
(After 1st line treatment)
p=0.01
Months of survival

Figure 3

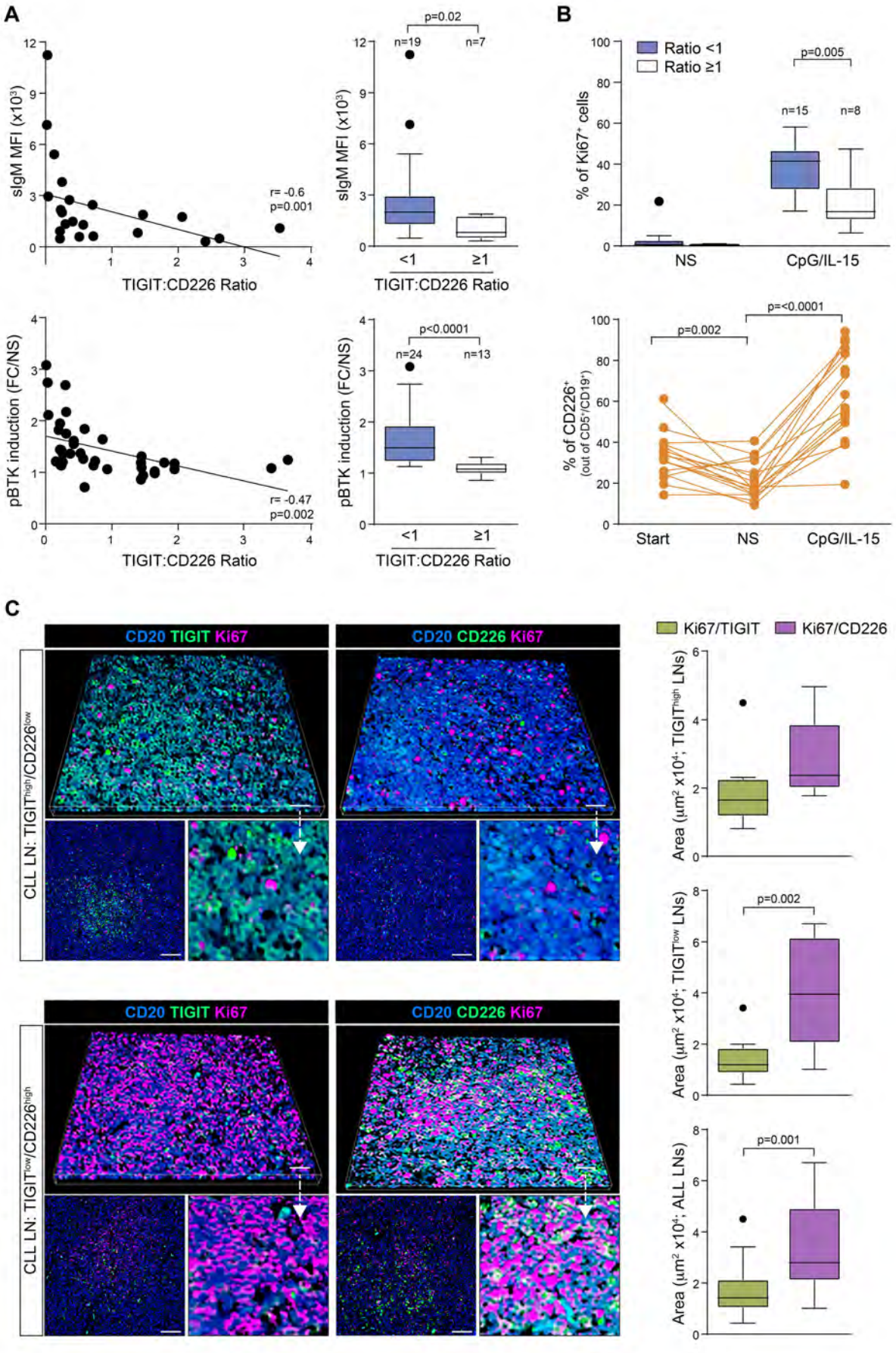
A
sIgM MFI (x10³)
TIGIT:CD226 Ratio
r= -0.6
p=0.001
p=0.02
n=19
n=7
<1
≥1
pBTK induction (FC/NS)
r= -0.47
p=0.002
p<0.0001
n=24
n=13
B
Ratio <1
Ratio ≥1
% of Ki67⁺ cells
p=0.005
n=15
n=8
NS
CpG/IL-15
% of CD226⁺ (out of CD5⁺/CD19⁺)
p=0.002
p=<0.0001
Start
C
CD20 TIGIT Ki67
CD20 CD226 Ki67
CLL LN: TIGIT^high/CD226^low
CLL LN: TIGIT^low/CD226^high
Ki67/TIGIT
Ki67/CD226
Area (µm² x10⁴; TIGIT^high LNs)
Area (µm² x10⁴; TIGIT^low LNs)
Area (µm² x10⁴; ALL LNs)
p=0.002
p=0.001

Figure 4

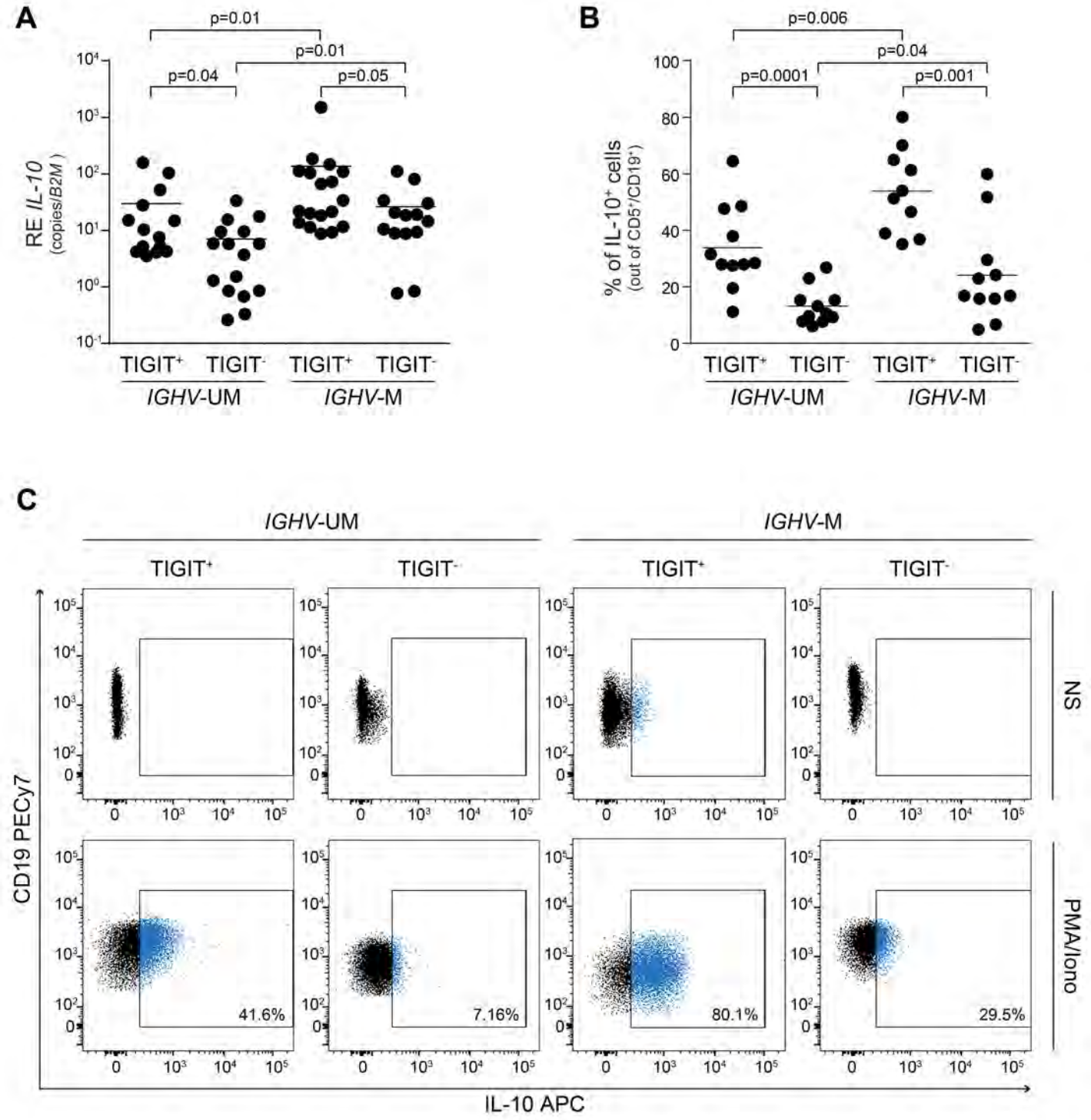
A
p=0.01
p=0.01
p=0.04
p=0.05
RE IL-10 (copies/B2M)
TIGIT+ TIGIT- TIGIT+ TIGIT-
IGHV-UM
IGHV-M
B
p=0.006
p=0.04
p=0.0001
p=0.001
% of IL-10+ cells (out of CD5+/CD19+)
TIGIT+ TIGIT- TIGIT+ TIGIT-
IGHV-UM
IGHV-M
C
IGHV-UM
IGHV-M
TIGIT+
TIGIT-
TIGIT+
TIGIT-
NS
PMA/Iono
41.6%
7.16%
80.1%
29.5%
CD19 PECy7
IL-10 APC

Figure 5

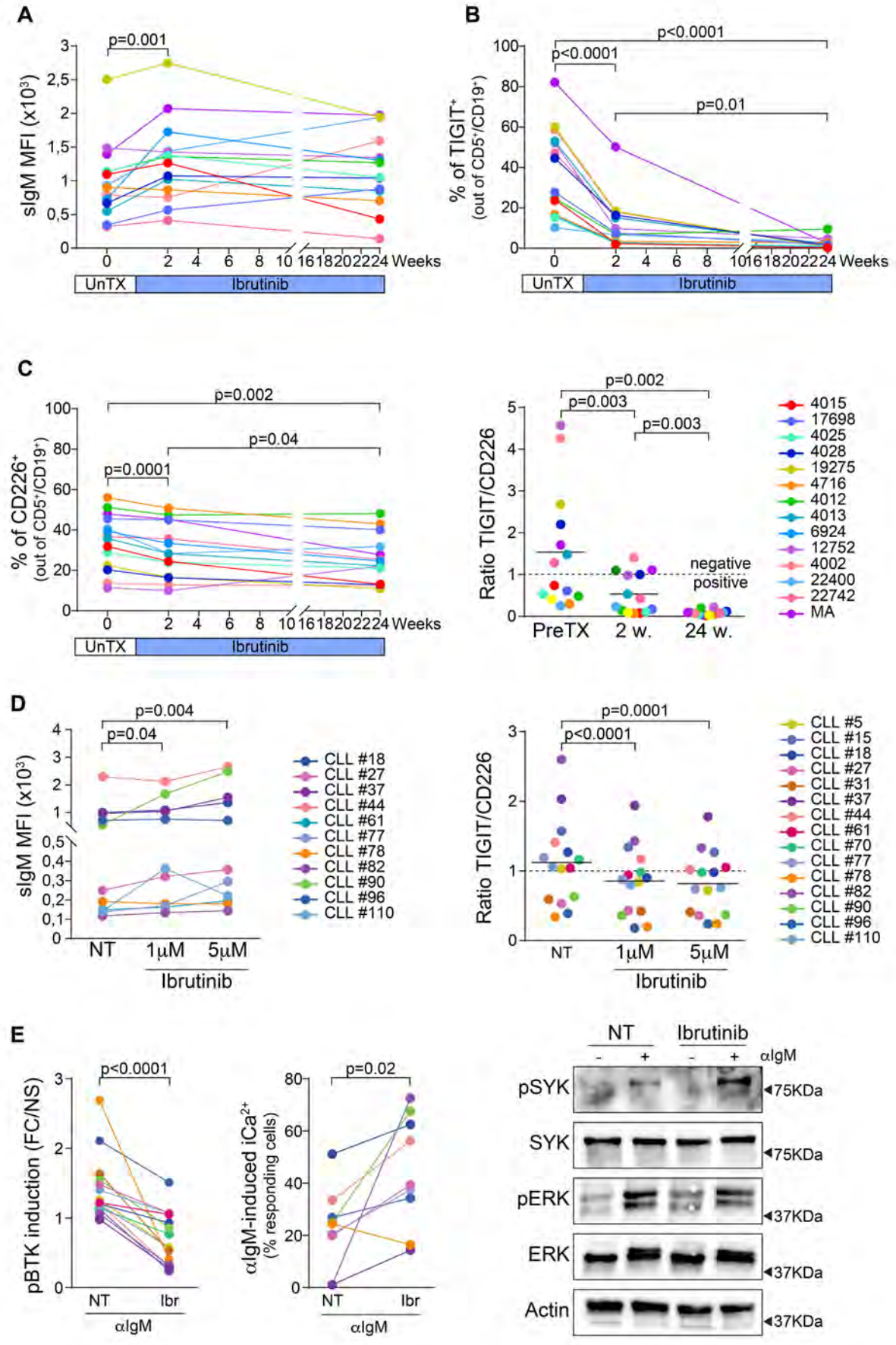
A
p=0.001
sIgM MFI (x10³)
Weeks
UnTX
Ibrutinib
B
p<0.0001
p<0.0001
p=0.01
% of TIGIT⁺ (out of CD5⁺/CD19⁺)
C
p=0.002
p=0.04
p=0.0001
% of CD226⁺ (out of CD5⁺/CD19⁺)
p=0.002
p=0.003
p=0.003
Ratio TIGIT/CD226
negative
positive
PreTX
2 w.
24 w.
4015
17698
4025
4028
19275
4716
4012
4013
6924
12752
4002
22400
22742
MA
D
p=0.004
p=0.04
sIgM MFI (x10³)
NT
1μM
5μM
Ibrutinib
CLL #18
CLL #27
CLL #37
CLL #44
CLL #61
CLL #77
CLL #78
CLL #82
CLL #90
CLL #96
CLL #110
p=0.0001
p<0.0001
Ratio TIGIT/CD226
CLL #5
CLL #15
CLL #18
CLL #27
CLL #31
CLL #37
CLL #44
CLL #61
CLL #70
CLL #77
CLL #78
CLL #82
CLL #90
CLL #96
CLL #110
E
p<0.0001
pBTK induction (FC/NS)
NT
Ibr
αIgM
p=0.02
αIgM-induced iCa²⁺ (% responding cells)
NT
Ibrutinib
αIgM
pSYK
SYK
pERK
ERK
Actin
75KDa
75KDa
37KDa
37KDa
37KDa

Figure 6

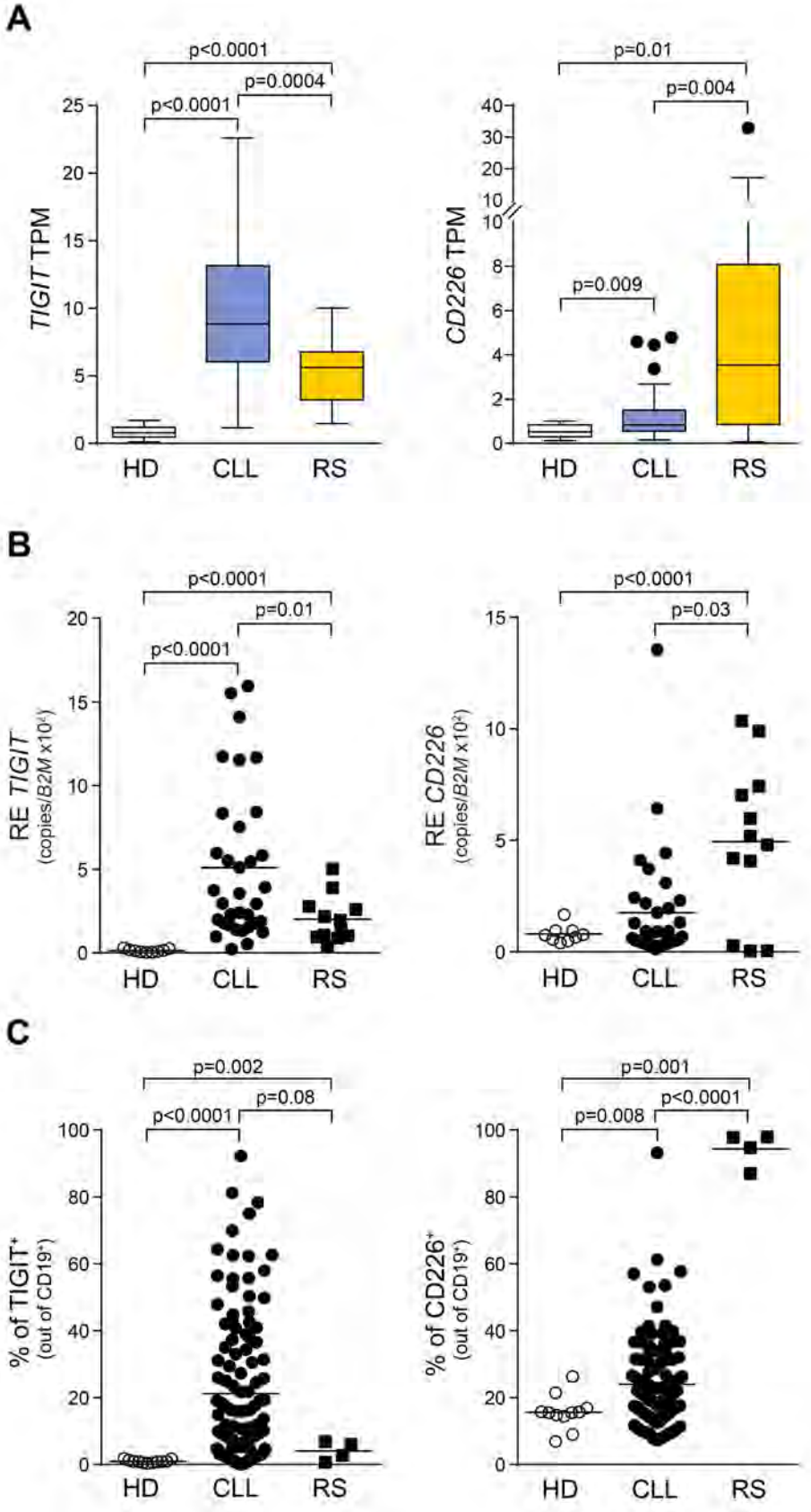
A
p<0.0001
p=0.0004
p<0.0001
TIGIT TPM
HD
CLL
RS
p=0.01
p=0.004
p=0.009
CD226 TPM
B
p<0.0001
p=0.01
p<0.0001
RE TIGIT (copies/B2M x10⁴)
p<0.0001
p=0.03
RE CD226 (copies/B2M x10⁴)
C
p=0.002
p=0.08
p<0.0001
% of TIGIT⁺ (out of CD19⁺)
p=0.001
p<0.0001
p=0.008
% of CD226⁺ (out of CD19⁺)

Figure 7

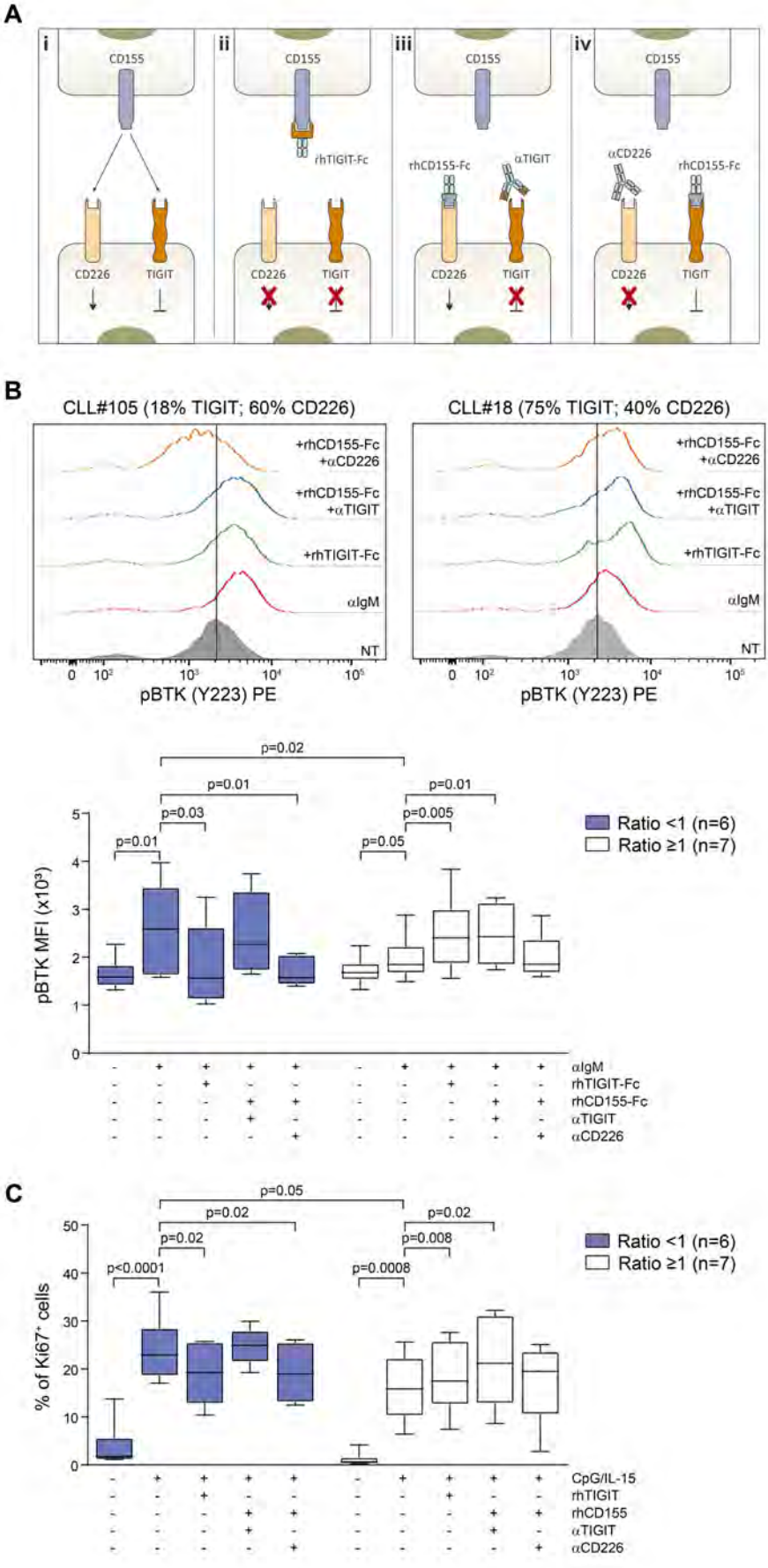
A
i
ii
iii
iv
CD155
CD226
TIGIT
rhTIGIT-Fc
rhCD155-Fc
αTIGIT
αCD226
B
CLL#105 (18% TIGIT; 60% CD226)
CLL#18 (75% TIGIT; 40% CD226)
+rhCD155-Fc +αCD226
+rhCD155-Fc +αTIGIT
+rhTIGIT-Fc
αIgM
NT
pBTK (Y223) PE
pBTK MFI (x10³)
p=0.02
p=0.01
p=0.03
p=0.005
p=0.05
Ratio <1 (n=6)
Ratio ≥1 (n=7)
αIgM
rhTIGIT-Fc
rhCD155-Fc
αTIGIT
αCD226
C
% of Ki67⁺ cells
p=0.05
p=0.02
p=0.008
p<0.0001
p=0.0008
CpG/IL-15
rhTIGIT
rhCD155
αTIGIT
αCD226

Supplemental Material

The TIGIT/CD226/CD155 immunomodulatory axis is deregulated in CLL and contributes to B-cell anergy

Francesca Arruga[1], Marta Rubin[1], Despoina Papazoglou[2], Andrea Iannello[1], Nikolaos Ioannou[2], Riccardo Moia[3], Davide Rossi[4], Gianluca Gaidano[3], Marta Coscia[5], Luca Laurenti[6], Giovanni D'Arena[7], John N. Allan[8], Richard R. Furman[8], Tiziana Vaisitti[1], Alan G. Ramsay[2] and Silvia Deaglio[1]

Supplemental methods

RNA extraction and qRT-PCR

RNA was extracted as described[1]. qRT-PCR was performed using the CFX384 instrument and analyzed with the CFX Maestro Software (Biorad). Primers for *TIGIT* (Hs00545087_m1), *CD226* (Hs00170832_m1), *CD155* (PVR, Hs00197846_m1), *IL10* (Hs00961622_m1) and *B2M* (Hs00984230_m1) were all from Thermofisher. The data were analyzed with the $2^{-\Delta\Delta Ct}$ method, to calculate the relative expression of the gene under analysis. For each gene, expression levels were computed as the difference (ΔCT) between the target gene CT and *B2M* CT. Values were normalized over those of Control RNA (Life Technologies, Thermofisher) (ΔΔCT), added in each experiment for calibration purposes, and expressed in linear or in logarithmic scale.

Multispectral IHC, confocal microscopy and image analysis

IHC studies were performed on CLL LN tissues (Figure 1A n=6; Figure 5B, n= 3 UM-CLL; n=3 M-CLL) and reactive LN controls (Figure 1A n=4), as described[2]. The clinical characteristics of patients with mutated and unmutated IGHVs are presented in supplemental Table 1. Briefly, 4-5 µm sections prepared from FFPE human tissues were deparaffinized prior to antigen retrieval in citrate buffer. After blocking (5% donkey serum), primary antibodies were incubated overnight at 4 °C. The primary antibodies used for this study are the following: goat anti-human CD20 (ab194970, Abcam), rat anti-human ki67 (ab156956, Abcam), rabbit anti-human TIGIT (A700-047, BETHYL), rabbit anti-human CD226 (A700-063, BETHYL). Following primary antibody incubation and washing steps (0.05% Triton PBS), secondary antibody (donkey) staining was performed for 1 h at room temperature. All secondary antibodies were obtained from Jackson Immunoresearch: DyLightTM 405 AffiniPure Donkey anti-goat, Alexa Fluor® 488 AffiniPure Donkey anti-rabbit, Alexa Fluor® 647 AffiniPure Donkey anti-rat. The specificity of staining was optimized and controlled by using appropriate dilutions of primary or secondary staining alone. Slides were sealed with coverslips using mounting solution FluorSaveTM reagent (Merck Millipore) and imaged within two days. Medial optical section images were captured with an A1R confocal microscope using a 20X objective with NIS-elements imaging software (Nikon). Detectors were set to detect an optimal signal below saturation limits. Fluorescence was acquired sequentially to prevent passage of

fluorescence from other channels (DU4 sequential acquisition). Image sets to be compared were acquired during the same session.

The percentage of LN $CD20^+$ CLL cells expressing TIGIT or CD226 in M or UM CLL cases was measured with the Imaris image analysis software v.9.7.2 (Bitplane). The surface tool was used to threshold the fluorescent signals and create two surfaces: i) $CD20^+$ cells (blue fluorescent channel) and ii) $CD20^+TIGIT^+$ / $CD20^+CD226^+$ (green fluorescent channel) double-positive cells (colocalization channel). For the B cell proliferation analysis (Ki67 expression), the area (μm^2) of the colocalization signal of $CD20^+TIGIT^+$ with Ki67 and $CD20^+CD226^+$ with Ki67 was calculated. Three-five confocal images from representative areas were analyzed per patient tissue sample.

Phosflow assay

Phosflow assay to evaluate BTK phosphorylation upon BCR stimulation was performed as described[3]. Briefly, CLL cells (10^6) were thawed and plated over night to let them recover from anergy due to *in vivo* chronic BCR stimulation. After that, 10^6 cells were stimulated with 5 μg/ml anti-IgM (αIgM, Southern Biotech) for 5 minutes at 37 °C. Where indicated, cells were pre-treated (1 hour, on ice) with 5 μg/ml rhTIGIT-Fc or with αTIGIT or αCD226 blocking monoclonal antibodies (5 μg/10^6 cells, 30 minutes on ice), followed by 1 hour with rhCD155-Fc (5 μg/ml), before αIgM stimulation.

CpG/IL-15 stimulation

Stimulation of CLL cells proliferation with CpG/IL-15 was performed as described[4]. Briefly, $5x10^5$ CLL cells were cultured in a 96-well plate in RPMI 10% FCS and stimulated with 0.2 μM CpG ODN2006 and 15ng/ml of IL-15 for 6 days (replenished every 2 days). After stimulation, cell were partly used for surface staining of TIGIT and CD226, performed as previously described, and partly fixed and permeabilized with ice-cold 70% ethanol to proceed with intracellular staining of Ki67, following manufacturer's instructions. Details for reagents used are listed in Supplemental table 4.

IL-10 production

To assess IL-10 production, CLL cells were stimulated and stained as previously described[5]. Briefly, 10^6 cells were stimulated with phorbol 12-myristate 13-acetate (PMA, 50ng/ml) and ionomycin (1μg/ml) for 5 hours at 37 °C in the presence of a protein transport inhibitor cocktail (Invitrogen Ebioscience, Thermofisher) to prevent IL-10 secretion by CLL cells. Cells were washed and surface staining with anti-CD5 BB515 and anti-CD19 PECy7 (both from BD Biosciences) was performed. After that, cells were fixed and permeabilized using the BD Cytofix/Cytoperm Fixation/Permeabilization kit (BD Biosciences) before staining with anti-IL10 APC (BD Biosciences).

References

1. Vaisitti T, Gaudino F, Ouk S, et al. Targeting metabolism and survival in chronic lymphocytic leukemia and Richter syndrome cells by a novel NF-kappaB inhibitor. Haematologica. 2017;102(11):1878-1889.
2. Ioannou N, Hagner PR, Stokes M, et al. Triggering interferon signaling in T cells with avadomide sensitizes CLL to anti-PD-L1/PD-1 immunotherapy. Blood. 2021;137(2):216-231.
3. Arruga F, Bracciama V, Vitale N, et al. Bidirectional linkage between the B-cell receptor and NOTCH1 in chronic lymphocytic leukemia and in Richter's syndrome: therapeutic implications. Leukemia. 2020;34(2):462-477.
4. Mongini PK, Gupta R, Boyle E, et al. TLR-9 and IL-15 Synergy Promotes the In Vitro Clonal Expansion of Chronic Lymphocytic Leukemia B Cells. J Immunol. 2015;195(3):901-923.
5. Drennan S, D'Avola A, Gao Y, et al. IL-10 production by CLL cells is enhanced in the anergic IGHV mutated subset and associates with reduced DNA methylation of the IL10 locus. Leukemia. 2017;31(8):1686-1694.

Supplemental Table1. CLL sample cohort. AGE= age at diagnosis; WBC= white blood cells (x10^3/μl); M=mutated; UM=unmutated; tri=trisomy; del=deletion.

SAMPLE ID	SEX	AGE	WBC	RAI	*IGHV*	FISH	*NOTCH1* mutations	CD5/CD19 (%)	$CD38^+$ (%)	$CD49d^+$ (%)	Notes
CLL #1	M	67	38,5	I	M	tri12; del11; del17	No	96,3	75,8	90,7	
CLL #2	F	51	17,7	I	UM	del13	No	92,5	35,9	34,9	*TP53* mut
CLL #3	M	61	63,3	I	M	del13	No	94,1	83,9	37,6	
CLL #4	M	79	24	0	M	del13	No	90,6	54,7	49,7	
CLL #5	F	56	17,2	0	M	del13	No	97,3	67,5	64,7	
CLL #6	M	65	61,3	II	M	del13	No	95,2	57,7	53,2	
CLL #7	M		4,7	0	UM	del11	No	98,4	75	48,4	
CLL #8	M		8,6	I	UM	del13	No	92	30,9	43,2	
CLL #9	F	61	16,9	0	UM	tri12	No	92,9	46,9	50,4	
CLL #10	M		5,4	I	M	tri12	No	98,9	55,8	76,4	
CLL #11	F	47	12,8	0	M	del13	No	87,3	49,6	42,7	
CLL #12	F	53	4,5	0	UM	tri12	Yes	59,5	49	59,4	
CLL #13	M	81		II	UM	normal	Yes	95,2	86,6	53,3	
CLL #14	M	69	18,7	II	M	del13	No	92,8	53,4	46,4	
CLL #15	F	65	480	0	UM	del13	Yes	96,6	51,5	79,5	
CLL #16	M	47	46,4	II	M	del13	No	92,8	48,4	61,9	
CLL #17	M	53	30,1	0	UM	del13	No	91,7	42,1	61,4	
CLL #18	M	55	14,9	0	UM	del13	No	96,1	62,6	55,8	
CLL #19	F		7,4	0	M	del13	No	74,7	41,5	34,9	
CLL #20	M		182,7	IV	UM	tri12; del17	No	93,6	45,7	68,6	
CLL #21	F	50	72,1	IV	M	tri12	No	92,8	91,9	93,6	
CLL #22	F	63	32,7	IV	UM	tri12	Yes	90,4	36,8	24,2	
CLL #23	M	49	56,5	II	UM	tri12	No	89,1	51,4	92,7	*TP53* mut
CLL #24	M	47	121,4	II	UM	tri12	Yes	94,7	25,3	50,4	
CLL #25	F		14,8	I	M	del13	No	94,5	31,9	15,7	

SAMPLE ID	SEX	AGE	WBC	RAI	*IGHV*	FISH	*NOTCH1* mutations	CD5/CD19 (%)	CD38^{+} (%)	CD49d^{+} (%)	Notes
CLL #26	F	65	43,4	I	M	normal	No	90,2	31,5	26,9	
CLL #27	F	65	69	II	M	normal	No	94,7	27,7	17,4	
CLL #28	M	67	16	0	M	del13	No	86,4	24,6	18	
CLL #29	M	79	14,8	III	UM	del11	No	95,7	66,5	29,4	
CLL #30	F	73	92	III	UM	tri12	No	82,5	84,1	97,6	
CLL #31	F		96,8	II	M	del13	No	88,8	37,3	30,2	
CLL #32	M	35	23	I	M	normal	No	79,4	30,5	14,3	
CLL #33	M	67	14,1	II	UM	tri12	Yes	92,1	82,7	61,6	
CLL #34	M	78	22,1	IV	UM	normal	No	96,8	40,9	54,2	
CLL #35	F	70	13	0	UM	normal	No	93,3	32,5	19,8	
CLL #36	M		8,7	II	UM	del13	No	69,7	73,7	95,3	
CLL #37	M	54		I	M	normal	No	96	51,3	87,8	
CLL #38	F	60	18	0	UM	normal	No	82,4	37,5	24,2	
CLL #39	M		13,3	I	UM	normal	No	91,4	9,1	1,1	
CLL #40	M	35		0	M	normal	No	93,2	41,6	37,5	
CLL #41	M	62	58	I	M	normal	No	95,8	34,8	26,7	
CLL #42	F	64	99,3	0	UM	del17	Yes	91,4	36,6	47,3	
CLL #43	M	50	23,1	II	M	tri12	No	81,9	29	73,2	
CLL #44	M	72	21,1	0	M	del13	No	72,7	20,4	10,4	
CLL #45	M		128	IV	M	del13	No	93,5	26,7	28,3	*TP53* mut
CLL #46	M	42	19,5	I	M	del13	No	84,4	18,3	17,9	
CLL #47	M	59	33	I	M	del17; del13	No	**99,6**	59,4	43,5	
CLL #48	M	51	175,1	II	M	normal	No	83,1	15,1	10,4	
CLL #49	F		32	I	UM	del13	No	90,1	22,6	31,3	*TP53* mut
CLL #50	M	64	31,1	I	UM	del13	No	84	19,5	16	
CLL #51				II	UM	del13	No	70,1	23,6	18,2	
CLL #52	M	73	38,2	0	M	normal	No	96,4	15	10,8	

SAMPLE ID	SEX	AGE	WBC	RAI	*IGHV*	FISH	*NOTCH1* mutations	CD5/CD19 (%)	CD38^{+} (%)	CD49d^{+} (%)	Notes
CLL #53	M	59	82,1	I	M	del13	No	87,5	19,3	19,1	
CLL #54	F	58	2,3	I	UM	del13	No	82,7	32,6	86,5	*TP53* mut
CLL #55	M	74	5,3	I	UM	del13	No	89,6	9,9	8,63	
CLL #56	M	66	1,7	I	UM	del13	No	92,4	44,6	14,7	
CLL #57	M	54	48,9	I	M	del13	No	90,5	22,6	67,9	*TP53* mut
CLL #58	F	77	3,5	0	M	normal	Yes	86,3	42,7	96,5	
CLL #59	F	80	1,5	0	UM	normal	Yes	96,1	3,2	13,7	
CLL #60	M	66		I	M	del13	No	93,1	0,2	8,21	
CLL #61	F	52	1	I	M	del13	No	84,5	0,1	8,11	
CLL #62	M	71	2	I	UM	del13	No	83	26,6	4,3	
CLL #63	F	63	1,6	I	M	del13	No	86,8	0,3	5,7	
CLL #64	F			0	M	normal	No	67,7	2,3	17,4	
CLL #65	M	82	3,2	0	UM	normal	No	76,8	2,5	37,8	
CLL #66	F	65	38	I	M	tri12	Yes	92,2	0,2	8,5	
CLL #67	M	63	80,2	II	M	normal	No	96,2	0,1	54,9	
CLL #68	M	53	15,7	I	M	del13	No	82,3	0,2	55,9	
CLL #69	F	82	36,3	I	M	del11	No	95	0,1	12	
CLL #70	F	74		I	M	del13	No	95,8	28,5	29,6	
CLL #71	F	50	28,8	I	UM	del13	tbd	91,2	0,2	28,6	
CLL #72	F	69	2,1	I	UM	del13	No	97,1	1	58,6	
CLL #73	F	69	2,3	I	M	del13	No	81,8	16	9,6	
CLL #74	M	62	1,1	0	UM	tri12	No	91,1	8	88,2	
CLL #75	M	55	3,3	I	M	del13	No	82,5	1	28,7	
CLL #76	M	52	21	0	UM	del13	No	98,3	78	23,7	
CLL #77	F	54	1,7	0	M	del13	No	80,5	17	31,4	
CLL #78	M	59	1,9	I	M	del13	No	84,2	1	20,5	
CLL #79	F		2	0	UM	del11	No	95,6	10	13,9	

SAMPLE ID	SEX	AGE	WBC	RAI	*IGHV*	FISH	*NOTCH1* mutations	CD5/CD19 (%)	CD38^{+} (%)	CD49d^{+} (%)	Notes
CLL #80	M	49	1,8	I	M	del13	No	81,8	16	11,6	
CLL #81	M	60	1,4	0	M	tri12	No	35,7	88	94,6	
CLL #82	M	61	61,7	I	M	del13	No	80,2	1,3	16,9	
CLL #83	F	63	30,6	0	UM	normal	No	90,5	4,3	14,2	
CLL #84	M	48	35,7	I	UM	del13	No	45	86,9	45,4	
CLL #85	F	42	40,1	I	UM	del13	No	90,4	79,3	98,3	
CLL #86	M	54	43,5	I	M	del13	No	95,2	1,8	16,7	
CLL #87	M	56	25,7	0	M	normal	No	91,6		15,6	*TP53* mut
CLL #88	M	63	76,8	IV	UM	del13	No	80,7	1	99,3	*TP53* mut
CLL #89	M	75	260	IV	UM	tri12	No	55	1,1	92,5	
CLL #90	F	64	221,9	II	UM	del13	No	98,2	76,9	29,7	
CLL #91	F	57	107,1	II	M	del13	No	92,2	0,8	0,1	
CLL #92	M	63	261	IV	UM	del11; del17	No	92,2	10,7	63,7	*TP53* mut
CLL #93	F	73	255,9	II	UM	normal	Yes	76,4	37	19	
CLL #94	F	47	41,7	IV	M	del13	No	94,5	1,5	4,6	
CLL #95	F	68	168,6	III	UM	tri12	ND	95,7	59,3	93,1	
CLL #96	M	58	65,4	II	UM	del13	No	93,8	72,9	70,8	
CLL #97	M	69	208	III	UM	del13	No	92,3	1,5	0,1	
CLL #98	M	57	115	IV	UM	del13	No	84,5	15,9	21,2	
CLL #99	M	54	222,4	III	UM	del13	Yes	95,5	85,3	65,3	
CLL #100	M	58	178,7	III	M	del13; del11	Yes	93,1	2,4	0,1	
CLL #101	M	61	278,1	IV	UM	del13; del11	No	96,1	27,9	4,6	*TP53* mut
CLL #102	M	35	80	I	UM	normal	No	95	40,5	19,1	
CLL #103	M	65		I	UM	normal	No	90	43,9	21,7	
CLL #104	M	75		I	UM	normal	Yes	90,7	75,8	14,6	
CLL #105	F	70	32,7	0	UM	del13	No	93,4	46,5	20,3	
CLL #106	F	65	92,8	I	UM	del13	Yes	94,8	40,3	26,8	

SAMPLE ID	SEX	AGE	WBC	RAI	*IGHV*	FISH	*NOTCH1* mutations	CD5/CD19 (%)	$CD38^+$ (%)	$CD49d^+$ (%)	Notes
CLL #107	M	60	24,8	I	UM	del11	Yes	88,2	43,9	31,6	
CLL #108	M	54	64,3	I	UM	del13	No	99,1	40,3	33,9	
CLL #109	F	56	49,5	0	UM	tri12	Yes	93,9	56,2	54,7	
CLL #110	F	58	31,1	0	UM	del13	No	85,6	36,1	9,9	
CLL #111	F	73	46,4	I	UM	tri12	Yes	72,7	70	93,2	
CLL #112	M	74	57,2	IV	UM	del13	Yes	89,9	45	31,9	
CLL #113	M	68	80,5	II	UM	del17	No	97,6	54,4	91,7	*TP53* mut
CLL #114	M		36,8	II	UM	del13	No	98,6	40	39,2	
CLL #115	F	74	31,6	0	M	del13	No	98,4	53,7	33	

Supplemental Table2. Features of CLL samples examined during the follow up of the disease. AGE= age at diagnosis; WBC= white blood cells (x10^3/μl); M=mutated; UM=unmutated; tri=trisomy; del=deletion.

SAMPLE ID	SEX	AGE	WBC	RAI	*IGHV*	FISH	*NOTCH1* mutations	CD5/CD19 (%)	$CD38^+$ (%)	$CD49d^+$ (%)	Notes
04015	M	46	11,4	IV	UM	del17	No	74,9	85,9	66,4	
17698	M	41	30	IV	ND	del11; del13	Yes	83,4	72,4	80	
04025	M	70	42	III	UM	del11	No	91,6	37,2	66,4	*TP53* mut
04028	M	77	25	IV	ND	del17	No	93,9	44,4	71	*TP53* mut
19275	M	70	8,4	I	M	normal	No	81	84,4	48,2	
4716	F	61	265	IV	UM	tri12	No	92,7	67,2	72,9	
04012	F	71	3,11	IV	UM	del17; del13	Yes	60,3	67,7	74,7	*TP53* mut
04013	M	72	38	II	M	del17; del13	No	94,7	47,9	49	*TP53* mut
6924	M	47	22,9	II	UM	del11; del13	No	84,7	54,8	44,5	
12752	M	81	9,62	I	UM	del13	No	48	71,1	23,8	
04002	F	64	102	I	UM	del17	No	79,2	10,5	4,55	*TP53* mut
22400	M	58	95	IV	UM	del11	No	82,9	61,3	48,9	
22742	M	65	14,5	II	M	del13	No	96,1	45,9	56,9	
MA	M	46	220	II	M	normal	No	97,2	42,2	96,8	

Supplemental Table 3. Features of CLL patients used for histologic analyses on LN biopsies.

SAMPLE ID	SEX	AGE	RAI/BINET	*IGHV*	FISH	$CD38^+$ (%)
CLL #1001	M	76	0/A	M	Normal	85
CLL #1002	M	64	1/A	M	del (13q)	0
CLL #1003	M	50	NK	M	NK	NK
CLL #1004	M	76	2/B	UM	del (13q)	60
CLL #1005	F	75	NK	UM	del (13q)	NK
CLL #1006	F	80	NK	UM	del (13q)	NK

*NK=not known

Supplemental Table 4. List of antibodies and reagents.

Reagent	Manufacturer
APC-R700 Mouse anti-Human CD5	BD Biosciences, Milan, Italy
BB515 Mouse anti-Human CD5	BD Biosciences, Milan, Italy
BV510 Mouse anti-Human CD19	BD Biosciences, Milan, Italy
PE-Cy7 Mouse anti-Human CD19	BD Biosciences, Milan, Italy
APC Mouse anti-Human CD73	BD Biosciences, Milan, Italy
BB515 Mouse anti-Human CD38	BD Biosciences, Milan, Italy
BV605 Mouse anti-Human CD49d	BD Biosciences, Milan, Italy
BV650 Mouse anti-Human CD3	BD Biosciences, Milan, Italy
APC-R700 Mouse anti-Human CD4	BD Biosciences, Milan, Italy
BV510 Mouse anti-Human CD8	BD Biosciences, Milan, Italy
APC-H7 Mouse anti-Human CD14	BD Biosciences, Milan, Italy
PE anti-human BTK (pTyr223)/ITK (pTyr180)	BD Biosciences, Milan, Italy
APC Mouse anti-Human IL-10	BD Biosciences, Milan, Italy
PE Mouse anti-Human IgM	BioLegend, San Diego, CA, USA
PE Mouse anti-Human TIGIT (Clone MBSA43)	Invitrogen Ebioscience, Thermofisher, Milan, Italy
PerCP-eFluor 710 Mouse anti-Human CD155 (Clone 2H7CD155)	Invitrogen Ebioscience, Thermofisher, Milan, Italy
PE-Vio770 Mouse anti-Human CD226 (DNAM1) (Clone DX11)	Miltenyi Biotec, Bologna, Italy
APC Anti-Human and -Mouse Ki-67	Miltenyi Biotec, Bologna, Italy
Recombinant Human TIGIT Fc Chimera Protein	R&D System, Bio-Techne SRL, Milan,Italy
Recombinant Human CD155/PVR Fc Chimera Protein	R&D System, Bio-Techne SRL, Milan,Italy
TIGIT Monoclonal Antibody (MBSA43), Functional Grade	Invitrogen Ebioscience, Thermofisher, Milan, Italy
CD226 (DNAM-1) Monoclonal Antibody (DX11)	Invitrogen Ebioscience, Thermofisher, Milan, Italy
Goat Anti-Human IgM-unlabeled	Southern Biotech, Birmingham, AL, USA
CpG ODN 2006	InvivoGen, Toulouse, France
Recombinant Human IL-15 Protein	R&D System, Bio-Techne SRL, Milan,Italy

Supplemental Table 5. Flow cytometry multiparametric strategy. FMO= Fluorescence Minus One.

Mix ID	Marker	Fluorochrome
FMO B_1	CD5	APC-R-700
	CD19	BV510
	IgM	PE
FMO B_2	CD5	APC-R-700
	CD19	BV510
	CD73	APC
	CD38	BB515
	CD49d	BV605
TIGIT panel B	CD5	APC-R-700
	CD19	BV510
	CD73	APC
	CD38	BB515
	CD49d	BV605
	TIGIT	PE
	CD155	PerCP-Cy5.5
	CD226	PE-Cy7
FMO T/Mono	CD3	BV650
	CD4	APC-R-700
	CD8	BV510
	CD14	APC-H7
TIGIT panel T/Mono	CD3	BV650
	CD4	APC-R-700
	CD8	BV510
	CD14	APC-H7
	TIGIT	PE
	CD155	PerCP-Cy5.5
	CD226	PE-Cy7

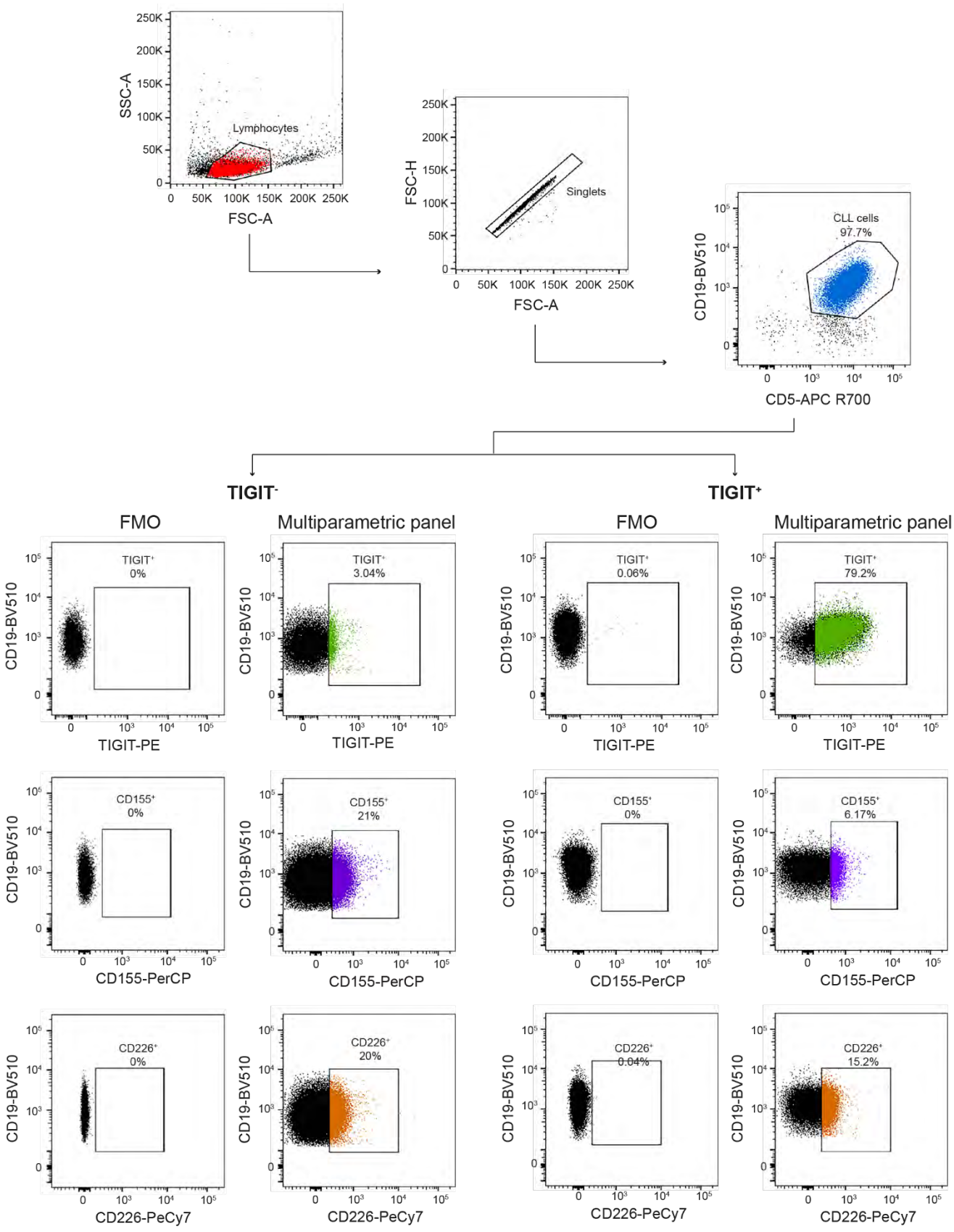

Supplemental Figure 1

Supplemental Figure 1. Flow cytometry gating strategy for B cells. Lymphocytes were morphologically gated and singlets were examined. B cells were isolated as $CD19^+/CD5^+$ cells (CLL cells) or $CD19^+$ cells (normal B lymphocytes). The gates for $TIGIT^+$, $CD226^+$ and $CD155^+$ cells were set based on the Fluorescence Minus One (FMO) to take into account the presence of multiple fluorochromes.

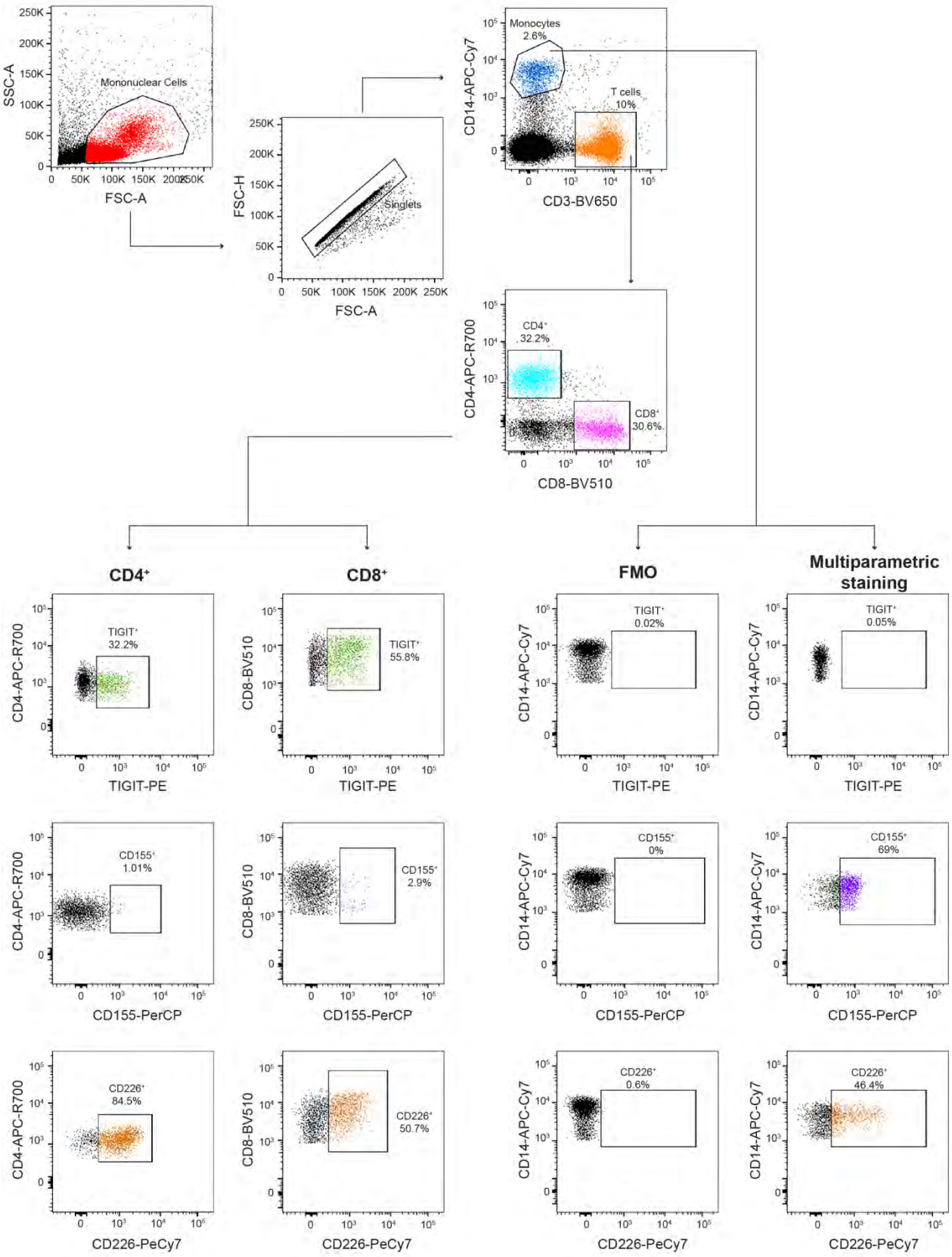

Supplemental Figure 2

Supplemental Figure 2. Flow cytometry gating strategy for T cells and monocytes. Mononuclear cells were morphologically gated and singlets were examined. T cells were defined as $CD3^+$ cells and further divided in $CD4^+$ and $CD8^+$ T lymphocytes, monocytes were defined as $CD14^+$ cells. For each subpopulation, gates for $TIGIT^+$, $CD226^+$ and $CD155^+$ cells were set based on the FMO (not shown for $CD4^+$ and $CD8^+$).

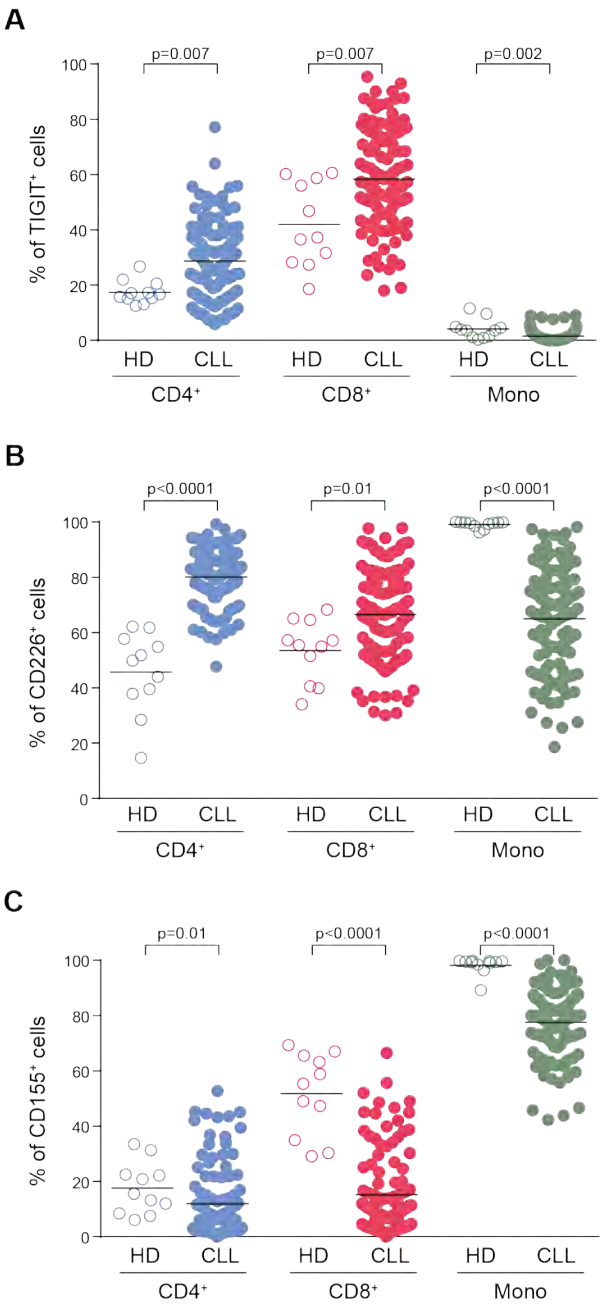

Supplemental Figure 3

Supplemental Figure 3. Expression of TIGIT, CD226 and CD155 on PBMC subpopulations. Flow cytometry analysis of TIGIT, CD226 and CD155 expression on CD4+ or CD8+ T lymphocytes and monocytes collected from CLL patients and healthy donors (HD).

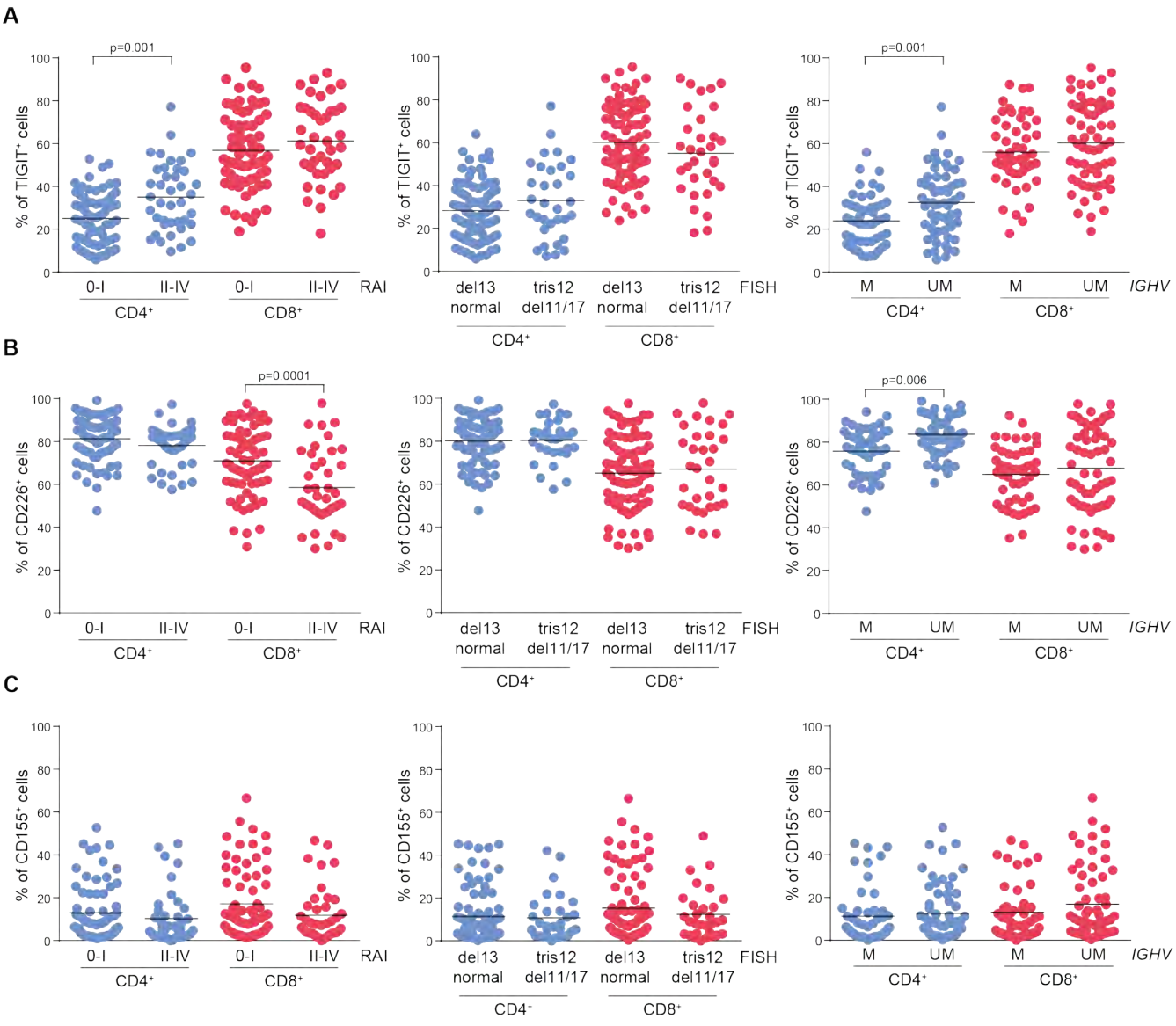

Supplemental Figure 4

Supplemental Figure 4. TIGIT axis in T lymphocytes from CLL patients. A. Flow cytometry analysis of surface TIGIT in $CD4^+$ and $CD8^+$ cells collected from CLL samples, divided according to prognostic markers (left: RAI; middle: cytogenetics; right: *IGHV* mutation). **B.** Flow cytometry analysis of surface CD226 in $CD4^+$ and $CD8^+$ cells collected from CLL samples, divided according to prognostic markers (left: RAI; middle: cytogenetics; right: *IGHV* mutation). **C.** Flow cytometry analysis of surface CD155 in $CD4^+$ and $CD8^+$ cells collected from CLL samples, divided according to prognostic markers (left: RAI; middle: cytogenetics; right: *IGHV* mutation).

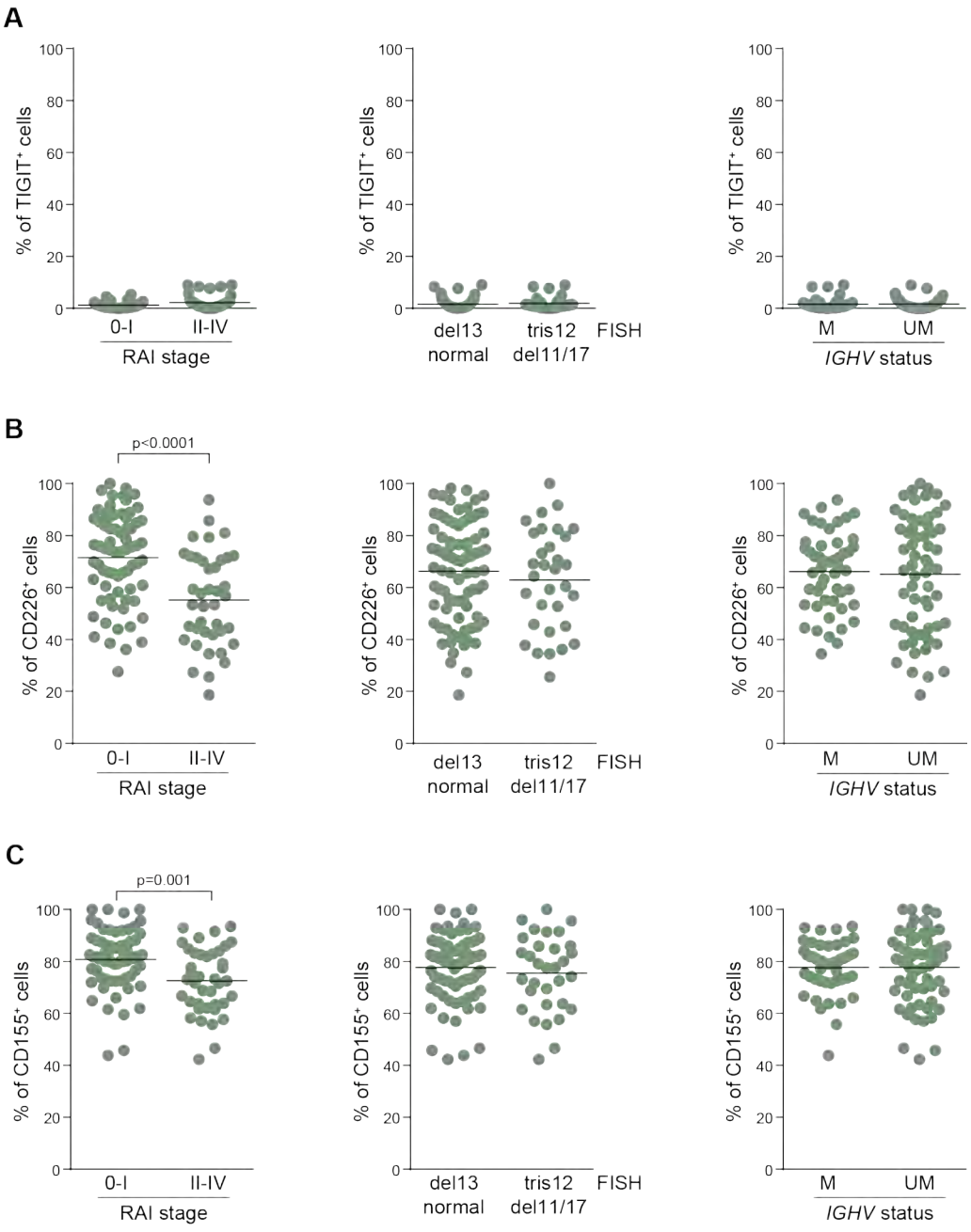

Supplemental Figure 5

Supplemental Figure 5. TIGIT axis in monocytes from CLL patients. A. Flow cytometry analysis of surface TIGIT in monocytes collected from CLL samples, divided according to prognostic markers (left: RAI; middle: cytogenetics; right: *IGHV* mutation). **B.** Flow cytometry analysis of surface CD226 in monocytes collected from CLL samples, divided according to prognostic markers (left: RAI; middle: cytogenetics; right: *IGHV* mutation). **C.** Flow cytometry analysis of surface CD155 in monocytes collected from CLL samples, divided according to prognostic markers (left: RAI; middle: cytogenetics; right: *IGHV* mutation).

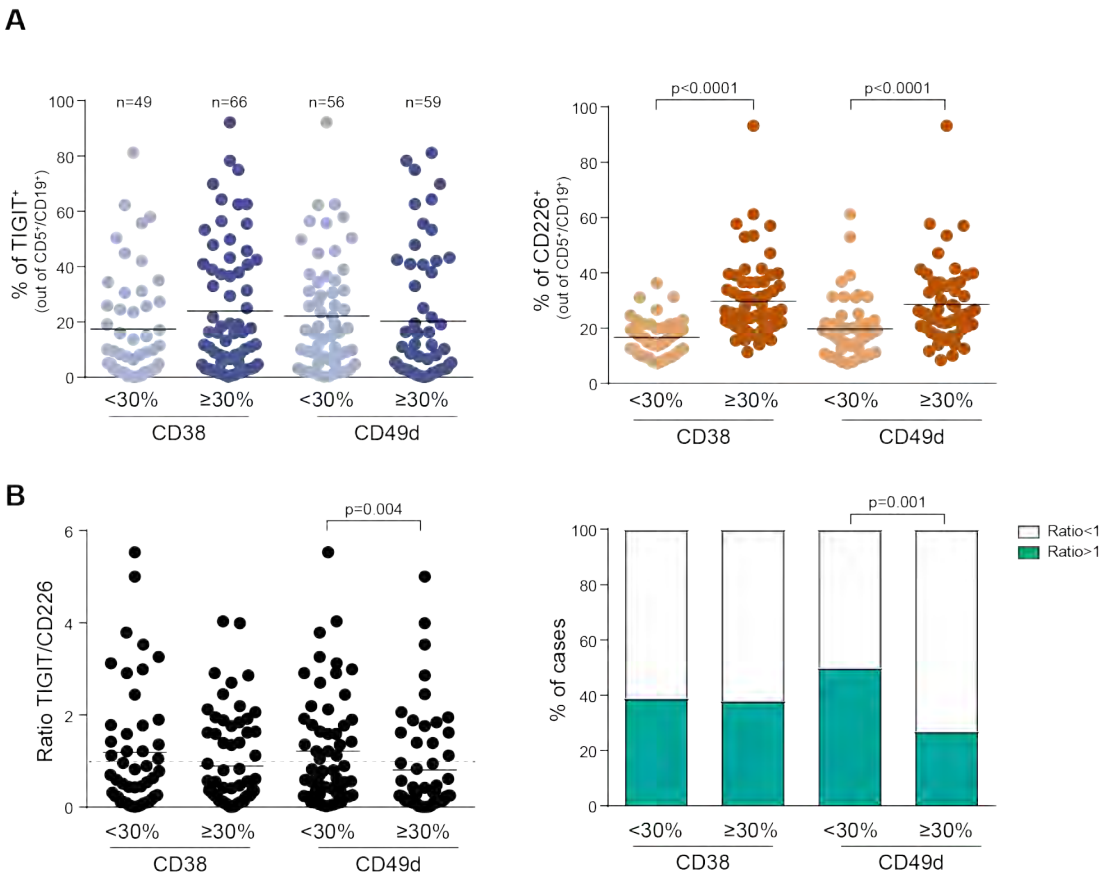

Supplemental Figure 6

Supplemental Figure 6. TIGIT and CD226 expression according to CD38 and CD49d. A. Percentages of TIGIT$^+$ and CD226$^+$ cells in CD38$^+$/CD38$^-$ and CD49d$^+$/CD49d$^-$ CLL samples (top panels); **B.** Dot plot showing TIGIT:CD226 ratio values for all the CLL samples divided according to the expression of CD38 and CD49d (left) and contingency plot indicating the enrichment of samples with ratio ≥1 or <1 in either prognostic category (right). Dashed line at Y=1 indicates the threshold to discriminate between negative signaling (TIGIT:CD226 ratio>1, prevalence of TIGIT) and positive signaling (TIGIT:CD226 ratio<1, prevalence of CD226).

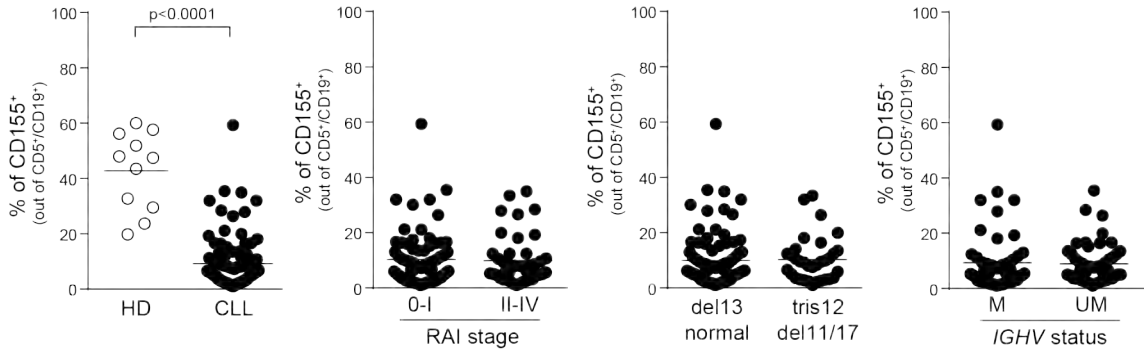

Supplemental Figure 7

Supplemental Figure 7. Expression of CD155. Flow cytometry analysis of surface CD155 expression in CLL samples compared to HD and correlation with CLL prognostic markers.

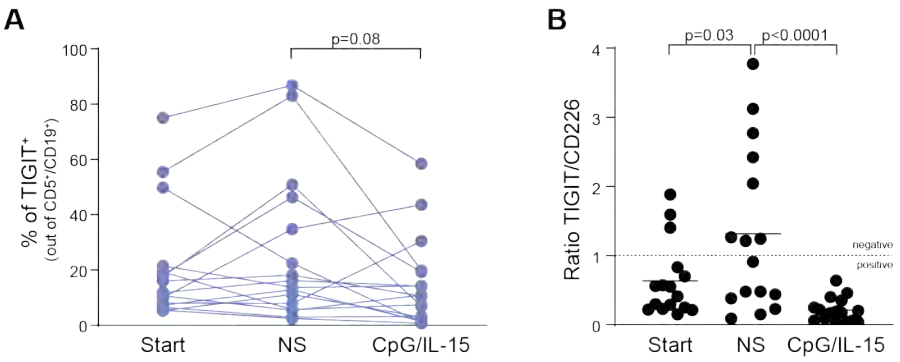

Supplemental Figure 8

Supplemental Figure 8. Modulation of TIGIT axis upon CpG/IL-15 culture. A. Flow cytometry analysis of TIGIT expression at the starting point and after 6 days of culture in the presence or absence of CpG/IL-15. **B.** Analysis of TIGIT:CD226 ratio at the starting point and after 6 days of culture in the presence or absence of CpG/IL-15. Dashed line at Y=1 indicates the threshold to discriminate between negative signaling (TIGIT:CD226 ratio>1, prevalence of TIGIT) and positive signaling (TIGIT:CD226 ratio<1, prevalence of CD226).

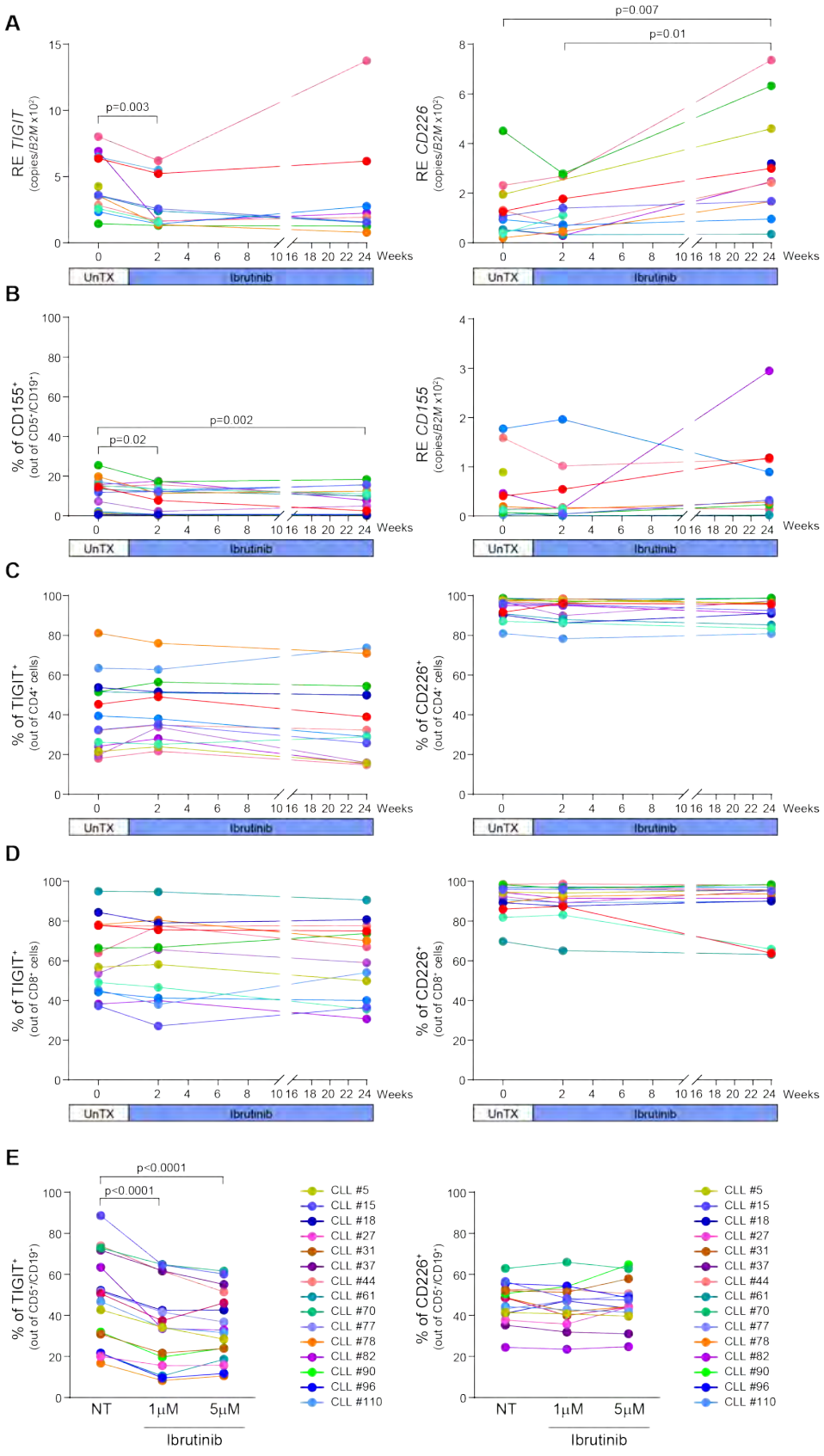

Supplemental Figure 9

Supplemental Figure 9. TIGIT, CD226 and CD155 during the follow up. A. qRT-PCR analysis of *TIGIT* and *CD226* expression in CLL samples collected before treatment initiation or after 2 weeks or 24 weeks of ibrutinib therapy. **B.** Flow cytometry (left) and qRT-PCR analysis (right) of CD155 expression in CLL samples collected before treatment initiation or after 2 weeks or 24 weeks of ibrutinib therapy. **C.** Flow cytometry analysis of TIGIT (left) and CD226 (right) on $CD4^+$ T cells collected from CLL samples during the follow up. **D.** Flow cytometry analysis of TIGIT (left) and CD226 (right) on $CD8^+$ T cells collected from CLL samples during the follow up. **E.** Flow cytometry analysis of the percentage of $TIGIT^+$ (left) and $CD226^+$ (right) leukemic cells in CLL samples treated *in vitro* with 1 ad 5 μM ibrutinib for 48 hours.

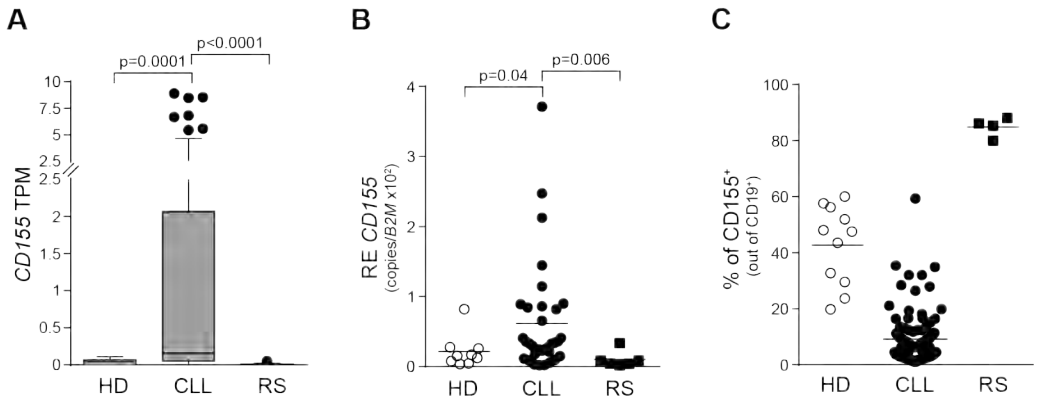

Supplemental Figure 10

Supplemental Figure 10. CD155 expression in RS. A. *CD155* TPM values in HD, CLL and primary RS samples. **B.** qRT-PCR validation of *CD155* expression in HD and CLL samples and in RS-PDX. **C.** Flow cytometry analysis of surface CD155 in HD and CLL samples and in RS-PDX.